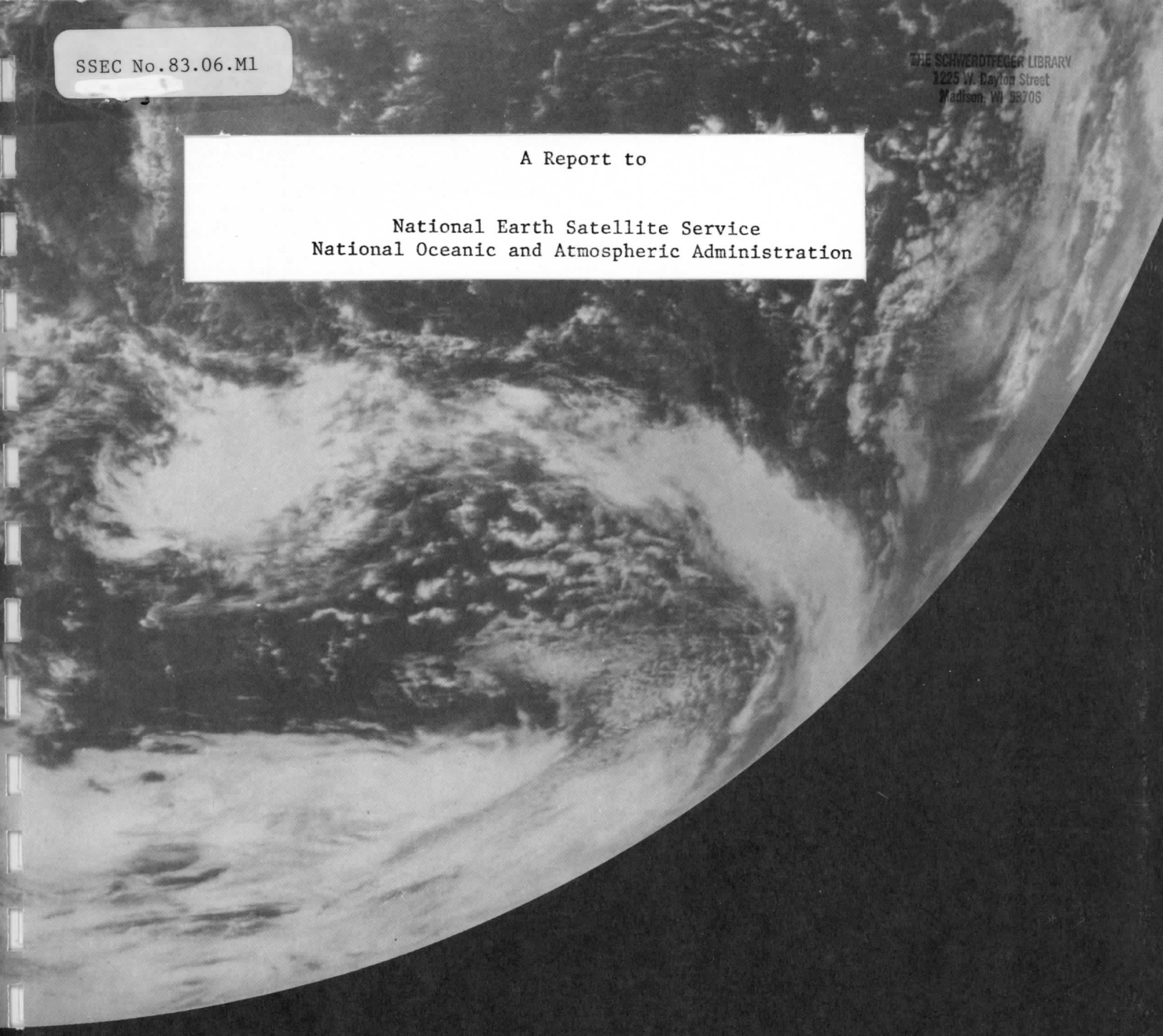

A Report to

National Earth Satellite Service
National Oceanic and Atmospheric Administration

# A REPORT

from the space science and engineering center
the university of wisconsin-madison
madison, wisconsin

A Report to

National Earth Satellite Service
National Oceanic and Atmospheric Administration

for

# The Development of Microwave Remote Sensing Techniques for the Measurement of Rainfall in Agricultural Areas

Contract #NA-80-SAC-00742
University of Wisconsin Account #144-P961

for the period of

1 Sept. 1980 to 30 April 1983

submitted by

David W. Martin

Roy W. Spencer

Space Science and Engineering Center

at the University of Wisconsin-Madison

1225 West Dayton Street

Madison, Wisconsin 53706

(608)262-0544

June, 1983

ABSTRACT

This report reviews the work done to date under contract #NA-80-SAC-00742 entitled "The Development of Microwave Remote Sensing Techniques for the Measurement of Rainfall in Agricultural Areas". Covered within are the primary accomplishments. These include the development of an algorithm to estimate rainfall from passive microwave observations of the Nimbus-7 Scanning Multichannel Microwave Radiometer (SMMR) over the central United States. Also discussed is a method to extend this information in time with the help of GOES visible and IR data.

Table of Contents

## 1. Introduction

Staff members at the University of Wisconsin-Madison were invited to participate in the NESS AgRISTARS program in the summer of 1979. In December of that year we submitted the proposal that led to the present project.

The 1979 proposal hinged on the use of satellite passive microwave data to infer rainfall over croplands. These were to be supplemented by data from visible and infrared imaging sensors to aid in interpolation between microwave passes. The work has been divided into two main tasks: (1) finding a microwave algorithm, and (2) improving the microwave rain estimates by means of visible or infrared observations.

Three proposals have been funded and worked under during this period, and are listed in Appendix 1.

## 2. Work done to date

### 2.1 Background

Early in the course of this work it was decided that a basic question to be answered was "how much information on rainfall is contained in the SMMR observations?" Answering this question required a "ground-truth", independent estimate of the rainfall to which we could compare the microwave data. We concluded that radar was the best candidate because, like SMMR, it views the atmosphere instantaneously and over spatially continuous areas. Because the signal we were searching for was expected to be small (e.g., see Atlas and Thiele, 1982), a large quantity of radar data was required. The WSR-57 radars operated by the National Weather Service, the displays of which are routinely photographed and archived, were chosen over isolated research radars. This choice was based upon the likelihood

of finding many SMMR-radar overlaps, and the broad crop region coverage provided by the WSR-57's.

2.2 SMMR

To evaluate the information contents of SMMR data, nine warm season orbits were processed. These covered parts of the United States between 4 May and 9 July, 1979. Selections were based on the extent of rain, as indicated in NWS radar summary charts, overlap of radar PPI photographs with SMMR swaths and coincidence in time (to within 5 minutes). Overlaying radar, SMMR, and GOES data required a common map base. Software was developed on the University of Wisconsin's Man-computer Interactive Data Access System (McIDAS) to display all of these products, in image format, in a GOES-east projection. Microfilm records of the radar displays were manually digitized into rain rates over a grid comparable to the SMMR 37 GHz channel resolution (~20 km).

Images of the SMMR and GOES data were displayed and navigated based on known landmarks. Errors in these data sometimes approached 20 km. The radar data, being accurate to within a few kilometers, were not adjusted. (Channel-by-channel comparisons of SMMR with radar data showed no addition of information by the 6.6 GHz H and V channels to that provided by the higher frequency channels; hence, the 6.6 GHz channels were discarded.) Next, the images were sampled on a 40 km grid and the resulting 4663 records of averaged infrared equivalent blackbody temperature, SMMR brightness temperature, and radar rain rates were entered into a stepwise regression procedure, with the radar rain rates as the dependent variable (predictand). Brightness temperatures for three SMMR channels (37V, 37H, 10.7H) of the eight used were found to have negative correlations with rain rate; i.e., these channels were responding mainly to rain-attenuated

radiation. The other channels had positive correlations with rain rate. They provide a measure of the land background (unattenuated) radiation. The GOES infrared data did not add significant additional rain information. These results are explained more fully in Spencer et al. (1983a, in Appendix 2).

The algorithm which resulted from this statistical procedure was found to explain 63% of the variance of the radar rain rates, and in an independent test explained 64%, an unexpectedly good performance.

Part of the reason for this success was the finding of 37 GHz brightness temperatures much lower (as low as 163 K) than those previously believed possible (e.g., Savage and Weinman, 1975). All cases of brightness temperatures less than 220 K were found to coincide with heavy rainfalls. These low temperatures can be explained theoretically by introducing precipitation-size ice hydrometeors into a layer above the (liquid) rain layer. The effect of the ice is to greatly reduce the brightness temperatures, observed from above, by backscattering some of the radiation upwelling from the liquid layer. Since the ice is typically present in greatest quantities within storms having strong updrafts, the lower brightness temperatures are naturally correlated with the heavier rain events. Evidence was also found for a possible correlation between the very low temperatures and severe weather occurrences. A more thorough discussion of these results is contained in Spencer et al. (1983b, in Appendix 3).

The difference in signs between high frequency coefficients and low frequency coefficients implies a sensitivity of rainrate to contrast in brightness temperature between the land background and the rain cells. The following explanation is suggested for this result. We know from

theory and observation that, given a constant land background temperature, for reasons already explained the lower the brightness temperature from the rain cell, the higher the rain rate. However, it was found that rain over warm land could have the same brightness temperature as a cold land surface. Thus, by taking into account variations in temperature of the land-atmosphere system, the contrast between land and rain cell temperatures provides more information on rain rate than do the rain attenuated temperatures alone. Additionally, the positive coefficients on the lower-frequency terms may reflect the presence of heavier rains within the warmer air masses.

Recent work (Spencer et al., 1983c, in Appendix 4) has addressed the role of footprint filling by the rain cells. As is known from earlier studies at 19 GHz (Austin and Geotis, 1978; Smith and Kidder, 1978; Medrow et al., 1982), plane parallel theory underestimates rain from a partly filled footprint. To maximize the contrast between rain cell radiation and background radiation, storms were analyzed over the radiatively cold Gulf of Mexico, within the range of coastal radars. The predictions of plane-parallel theory could not be reproduced even when beam filling was estimated by radar and then taken into account in the microwave observations. A partial explanation might lie in the shape of the raindrops, which is usually assumed to be spherical (e.g., Savage, 1976; Weinman and Guetter, 1977; Rodgers et al., 1979). Observations of the largest and broadest storms over the ocean (and thus those that obscure the ocean surface) showed that the radiation emanating from rain is always polarized, probably due to a preferred oblate spheriodal shape of larger drops. Radiation scattered out the sides of finite clouds might also help account for the observed discrepancies (Weinman and Davies, 1978). It was

concluded, based upon the polarization and size characteristics of a limited number of radar and SMMR observed storms, that the ∿20 km footprint of SMMR at 37 GHz is seldom covered by rain during the warm season, and thus plane-parallel theory probably does not produce accurate rain estimates over showery regions of the oceans. How this affects rain estimation over land is still unclear.

2.3 Visible-Infrared

It had been thought that a life history technique, like that of Stout, Martin, and Sikdar (1979), could be adapted to fill gaps between successive microwave passes. Because of the difficulty of following clouds in satellite picture sequences for a crop forecasting system, this proved to be impractical.

As an alternative, we have been experimenting with a technique, called grid history, which combines the best features of life history and indexing techniques. Grid history works over a movable, geographically defined array of points. Both the size of the array and its resolution are variable. Although rain rates are inferred for a time coresponding to a GOES visible and/or infrared image, the deduction depends directly upon trends deduced from an earlier or later image. The design of this technique has been described by Martin and Howland (1982, Appendix 5). In a test over the Arabian Sea (for a separate project; Martin and Howland, 1983), grid history has proven to be capable of resolving three intensities of daily rain rate (light, moderate, and heavy). Presently, a student, Elen Cutrim, is applying the technique (in the context of monthly estimates) to rainfall over Amazonia. A second student, Bonita Lee, is attempting to further automate the technique by assessing four dozen programmed pattern recognition algorithms related to intensity and texture.

The success of SMMR in predicting rain rate suggests use of the (presumed) twice daily microwave observations to establish rain rate thresholds for coincident, colocated infrared images. To impose some stability, probably the algorithm setting these thresholds would contain a memory. A version of grid history, more fully automated than at present, would use these thresholds to estimate, with manual oversight, rain rates intermediate in time (or space) to microwave passes.

## 3. Summary and plans

Our work to date has established the usefulness of passive microwave observations in the measurement of instantaneous rain rates over land during the warm season. Remaining tasks include similar studies for the spring and fall, and the integration of GOES and SMMR data to estimate daily rainfall. These tasks will be performed on the final year of AgRISTARS funding of the proposal entitled "Refining and Testing a Satellite Microwave Technique for Measurement of Rainfall over Croplands".

## 4. References


Atlas, D., and D.W. Thiele, 1982: Precipitation measurements from space: Workshop summary. Bull. Amer. Meteor. Soc., 63, 59-63.

Austin, P. M., and S. G. Geotis, 1978: Evaluation of the quality of precipitation data from a satellite-borne radiometer. Final report under NASA Grant NSG 5024. Department of Meteorology, Massachusetts Institute of Technology, Cambridge, Massachusetts, 02139.

Martin, D.W., and M.R. Howland, 1982: Rainfall over the Arabian Sea during the onset of the 1979 monsoon. Nature, 295, 628-629.

Martin, D.W. and M.R. Howland, 1983: Daily Arabian Sea rainfall during the onset of the 1979 monsoon. To be submitted to Papers in Meteorological Research.

Medrow, W., E. Raschke, and E. Ruprecht, 1982: Rainfall rates derived from Nimbus-5 observations analyzed against radar rainfall. Preprint, Sumposium uber Strahlungstransportprobleme und Satellitenmessungen in der Meteorologie und der Ozeanographie, Koin, 22-26 March. Deutscher Wetterdienst, Offenbach am Main, Fed. Rep. of Germany, 71-73.

Rodgers, E., H. Siddalingaigh, A. T. C. Chang, and T. Wilheit, 1979: A statistical technique for determining rainfall over land employing Nimbus 6 ESMR measurements. J. Appl. Meteor. 18, 978-991.

Savage, R.C. and J.A. Weinman, 1975: Preliminary calculations of the upwelling radiance from rain clouds at 37.0 and 19.35 GHz. Bull. Amer. Meteorol. Soc., 56, 1272-1274.

Savage, R. C., 1976: The Transfer of Thermal Microwaves Through Hydrometeors. Ph.D. Thesis, Dept. of Meteorology, Univ. of Wisconsin, Madison, 147 pp.

Smith, E. A., and S. Q. Kidder, 1978: A multispectral satellite approach to rainfall estimates. Department of Atmospheric Science, Colorado State University, Fort Collins, CO 80523.

Spencer, R. W., D. W. Martin, B. B. Hinton, and J. A. Weinman, 1983a: Satellite microwave radiances correlated with radar rain rates over land. Accepted for publication in Nature.

Spencer, R. W., W. S. Olson, Wu Rongzhang, D. W. Martin, J. A. Weinman, and D. A. Santek, 1983b: Heavy thunderstorms observed over land by the Nimbus-7 Scanning Multichannel Microwave Radiometer. Accepted for publication in Journal of Climatology and Applied Meteorology, 1983.

Spencer, R. W., B. B. Hinton, and W. S. Olson, 1983c: Nimbus-7 37 GHz radiances correlated with radar rain rates over the Gulf of Mexico. Submitted to Journal of Climatology and Applied Meteorology.

Stout, J. E., D. W. Martin, and D. N. Sikdar, 1979: Estimating GATE rainfall with geosynchronous satellite images. Mon. Wea. Rev., 107, 585-598.

Weinman, J. A., and R. Davies, 1978: Thermal microwave radiances from horizontally finite clouds of hydrometeors. J. Geophys. Res., 83, 3099-3107.

Weinman, J. A., and P. J. Guetter, 1977: Determination of rainfall distributions from microwave radiation measured by the Nimbus-6 ESMR. J. Appl. Meteor., 16, 437-442.

Appendix 1

Proposals Supporting the UW-Madison Microwave Land Rainfall Project

The Development of Microwave Remote Sensing Techniques for the Measurement of Rainfall in Agricultural Areas (December 1979 and January 1981)

A Demonstration of a Satellite Microwave Technique for the Measurement of Rainfall in Agricultural Areas (February 1982).

APPENDIX 2

# SATELLITE MICROWAVE RADIANCES CORRELATED WITH RADAR RAIN RATES OVER LAND

by

R.W. Spencer, D.W. Martin, B.B. Hinton, and J.A. Weinman

Space Science and Engineering Center
The University of Wisconsin-Madison
Madison, Wisconsin 53706 U.S.A

Submitted to Nature

February 1983

Satellite methods for the measurement of precipitation have employed images obtained at visible, infrared and microwave frequencies. Visible/infrared methods infer precipitation from the appearance and behavior of clouds. Microwave methods are more direct because the microwave radiation upwelling from the earth is affected more by rain drops than by cloud droplets. These radiances viewed by a sensor outside the atmosphere are presented as brightness temperature, the product of the thermodynamic temperature and emissivity of the surface viewed, modified by the intervening atmospheric constituents (water droplets, water vapor, gaseous absorption, etc.).

The radiative transfer calculations of Savage and Weinman[1] for a rain cloud over land show that the upwelling radiation at 37 GHz should be sensitive to changes in rain rate up to rates of 20 mm $hr^{-1}$. When the earth is viewed obliquely in vertical and horizontal polarizations, the radiation from standing water is highly polarized (wet soil and vegetation somewhat less so) whereas radiation from a rain cloud is only slightly polarized. Thus, as Weinman and Guetter[2] and Rodgers et al.[3] demonstrated, it is possible to distinguish between rain, lakes, and dry ground at 37 GHz. However, Rodgers et al. also found that it is difficult to distinguish between rain and wet ground. Furthermore, dew covered vegetation had the appearance of rain, and all distinctions between rain, wet land, dry land, and water disappeared for surface temperatures between 5°C and 15°C. Partly because of these results--which were obtained from a single frequency (37 GHz)--and partly because the emissivity of land at microwave frequencies ranges over a factor of two, the prospects of measuring rain rate over the continents by means of satellite-borne microwave radiometers generally had been discounted[4,5].

A recent instrument, the Scanning Multichannel Microwave Radiometer (SMMR)[6] on the Nimbus 7 and Seasat satellites measures radiation at 37 GHz and several additional frequencies. The SMMR measures perpendicularly polarized antenna temperatures at five frequencies, namely 37, 21, 18, 10.7 and 6.6 GHz. Its scan along a conical surface results in a constant incidence angle of $50^{o}$ at the surface of the earth. Horizontal resolution at the earth varies from a roughly circular footprint of approximately 20 km diameter at 37 GHz (a slight improvement over previous instruments) to about 70 km at 10.7 GHz. Rodgers et al.[7] successfully distinguished between rain, wet ground, and dry ground in data from SMMR for several orbital passes over the United States when data at 37, 18, and 10.7 GHz were utilized, and when surface temperatures were greater than 15°C. Taking their work one step further, rain rates derived from weather radar have been compared with brightness temperatures measured by the Nimbus 7 SMMR. In data collected over the central United States during the warm season, microwave radiances have been found to explain a relatively large percentage of the variance of the radar rain rates, over a range of rates previously thought to be not possible.

Like SMMR, radars provide an instantaneous view over large, spatially continuous areas. The WSR-57 radars in the U.S. National Weather Service network are maintained according to uniform procedures[8], including calibration checks made weekly or when there is a threat of severe weather. Radar plan position indicator (PPI) photographs are taken routinely and archived on microfilm. Relationships between the radar observed reflectivities and rain rates have been adopted for these radars based upon theory and extensive observation. The six reflectivity levels displayed by the WSR-57 were assigned average rain rates[8] of 4, 17, 42, 85, 147, and 190

mm $hr^{-1}$. The errors in rain rates inferred from radar measurements are caused by differing reflectivity-rain rate relationships among and even within storms, calibration changes, radar beam height change with distance from the transmitter, attenuation of the radar beam by heavy rain, evaporation of rain, rain traveling with the wind before reaching the ground, and false echoes due to anomalous propagation. These errors restrict the typical accuracy of radar rain rate measurements by research radars to a factor of two[9]. Nevertheless, for comparison with SMMR data, the temporal and spatial sampling similarities between the SMMR and the WSR-57 outweigh any advantage in point accuracy afforded by available networks of rain gages. Hence, the present study only considers rain rates inferred from WSR-57 radars.

PPI pictures were inspected on a microfilm reader. To be selected for digitizing, a picture had to show good time continuity of echo movement (thus excluding most cases of anomalous propagation), have an antenna elevation angle of less than 2 degrees, and be properly exposed. Only data within 230 km of the radar site were included. Most of the digitized pictures were taken within three minutes of the SMMR observation times; all were within six minutes.

Selected pictures were registered on a 20 km grid. The fraction of each 20 x 20 km bin covered by each intensity level was visually estimated and the corresponding rain rates were weighted by areal coverage to get an average bin rain rate. Based upon the operational nature of the WSR-57's, inter-radar differences, and the manual digitization of varying quality photographs of radar scopes that display only six discrete reflectivity levels, most of the resulting rain rates are within an error range of ±60%.

The analysis included data from the region east of the Rocky Mountains and west of the Appalachian Mountains. We chose one satellite orbit from early May, and eight orbits from a three week period during late June and early July of 1979. Four of the nine orbital passes occurred near local noon, and five near midnight. The orbit times chosen coincided with the most active rain systems during the period, ensuring that a significant number of rain storms would be available, as there was always an ample number of cases with no rain.

Microwave brightness temperatures and the digitized radar rain rates were entered into the University of Wisconsin's Man-computer Interactive Data Access System McIDAS[10]. SMMR data displayed as an image on a TV screen were checked for correct geographic placement, using the contrast at 37 GHz between water bodies and land as a guide. The largest repositioning of the data did not exceed one 37 GHz footprint (20 km). Fig. 1a is an example of a 37 GHz vertically polarized image over the central United States. Several cold (bright) areas resemble rain areas in the corresponding radar image (Fig. 1b). Other cold spots correspond to lakes and the Gulf of Mexico. Fig. 2 shows a composited radar image of all of the rain systems included in the analysis. The brightest areas correspond to the heaviest rain rates (up to 80 mm $hr^{-1}$).

Image sets consisting of the SMMR and digitized radar rainfall data were sampled on a 40 x 40 km grid. Only data within the digitized radar scans were included. A 40 km grid area average was calculated from each image, resulting in a set of 4663 "records", each consisting of averaged SMMR and radar data.

Rain never occurred in these warm season cases when the horizontally polarized 37 GHz brightness temperature was above 280 K. Also, cases of wet land or water bodies could be screened out by accepting only those records with a polarization difference between the vertical and horizontal 37 GHz averages that was less than 15°C. Lastly, microwave data at 37 GHz were found to be approximately linearly related to rain rate, with the lower brightness temperatures corresponding to the heavier rain rates. This linear relationship held for rain rates up to at least 40 mm $hr^{-1}$, due to unusually low brightness temperatures associated with the heavier rain rates. Spencer et al.[11] found that the cold 37 GHz temperatures (as low as 163 K) are probably due to backscattering of upwelling radiation by a layer of large ice particles. This layer is created and supported by strong thunderstorm updrafts, a condition required for the production of heavy rain. A similar result has been found in aircraft data obtained at 92 GHz[12,13].

A stepwise multiple linear regression procedure[14] was used to explore the extent to which the various channels were capable of supplying independent rain rate information. The rain rate, R, derived from microwave brightness temperatures, $T_i$, can be given by

$$R = a_o + \sum_{i=1}^{7} a_i T_i. \qquad (1)$$

The parameters derived from this regression analysis are shown in Table 1. Those terms with negative coefficients (37V, 37H, 10H) provide information on upwelling radiation from land that is attenuated by rain. Terms with positive coefficients (21V, 21H, 18V, 18H) represent a measure of the land

| Index $i$ | Frequency (GHz) | Polarization | Coefficient $a_i$ | Multiple Correlation Coefficient | % Variance Explained |
|---|---|---|---|---|---|
| 0 | | | 32.7 | | |
| 1 | 37 | V | -.363 | .579 | 34 |
| 2 | 21 | V | .172 | .710 | 50 |
| 3 | 21 | H | .200 | .724 | 52 |
| 4 | 37 | H | -.414 | .759 | 58 |
| 5 | 18 | V | .116 | .763 | 58 |
| 6 | 10 | H | -.214 | .772 | 60 |
| 7 | 18 | H | .385 | .790 | 62 |

Table 1. Variables in the order chosen by the stepwise regression procedure. Also shown are the coefficients of the regression equation. The units of $a_o$ are mm/hr and all other $a_i$'s have units of mm/hr K. Only those data where the 37 GHz polarization was less than 15°C and where the 37 GHz horizontal brightness temperature was less than 280 K are included, leaving a sample of 3813 cases.

background temperature in the vicinity of the rain cell. The brightness temperatures represented by these terms respond less to radiation from rain because the radiometers have coarser spatial resolution and measure radiation at longer wavelengths compared to the drop size of rain. Both rain-attenuated and land background brightness temperature measurements are needed because the estimate of rainfall is based upon the extent to which the radiation from land is attenuated by the rain. A display of the radar-measured and algorithm-estimated rain rates for the training data set (Fig. 3) illustrates the ranges of rain rate that were involved in the algorithm development. Note that of the 3813 data points, three radar observed cases of rain rate between 40 and 50 mm $hr^{-1}$ were not well explained by the microwave data. However, Spencer et al.[11] found that 37 GHz observations on a smaller spatial scale (400 $km^2$) were generally able to distinguish rain rates well above 40 mm $hr^{-1}$ in conjunction with heavy thunderstorms. The multiple correlation coefficient of this algorithm is 0.79. Considering the errors inherent in the manual digitization of radar PPI scope photographs, this is a remarkable result. It was found that an insignificant increase in correlation resulted from inclusion of nonlinear terms in the regression procedure.

We applied this algorithm to an independent set of SMMR data observed at the time represented in Fig. 1. At the outset of the study these data had been set aside for verification. SMMR-derived rain rates were compared to the corresponding radar rain rates shown in Fig. 1b. The relationship between the radar observed and microwave predicted rain rates is shown in Fig. 4. Note that the algorithm slightly underestimates the rain intensity at higher rain rates for this test data set. Also shown in Fig. 4 is a frequency histogram of the algorithm-predicted rain rates for radar rain

rates of zero. Most over-estimates are less than 1.5 mm/hr. The under-estimates would be set to zero in any operational use of the algorithm; however they illustrate the range of uncertainty that can be expected in low rain rate cases. A correlation coefficient of 0.80 for this independent test illustrates the algorithm's usefulness in estimating quantitative rain rates over land during the warm season.

Whether the relationship found here applies to other regions or times of the year remains to be investigated. However valid Eq. 1 might be, the sampling frequency of the current observing system on Nimbus 7 (twice per day, every other day) is not sufficient for the routine measurement of daily rainfall. Nevertheless, our results suggest that with more frequent microwave observations, either from additional polar orbiters or a geostationary satellite, passive microwave would move to front runner rank among satellite rain estimation techniques.

Acknowledgements. Funding for this study was provided by the National Oceanic and Atmospheric Administration National Earth Satellite Service through Grant NA-80-SAC-00742 and the National Aeronautics and Space Administration through Grant NAGW-380. SMMR data were provided by Per Gloersen and William Abbott of the Goddard Space Flight Center; their cooperation is appreciated. McIDAS programming assistance was provided by David Santek. The manuscript was typed by Angela Crowell.

References


1. Savage, R. C. and Weinman, J. A. Bull. Amer. Meteor. Soc. 56, 1272-1274 (1975).

2. Weinman, J. A. and Guetter, P. J. J. Appl. Meteor. 16, 437-442 (1977).

3. Rodgers, E., Siddalingaiah, H., Chang, A. T. C., and Wilheit, T. J. Appl. Meteor. 18, 978-991 (1979).

4. Atlas, D. and Thiele, O. Bull. Amer. Meteor. Soc. 63, 59-63 (1982).

5. Barrett, E. C. and Martin, D. W. The Use of Satellite Data in Rainfall Monitoring. Academic Press, London, 301-311 (1981).

6. Gloersen, P. and Hardis, L. The Nimbus 7 Users' Guide. National Aeronautics and Space Administration, Greenbelt, Maryland, 213-245 (1978).

7. Rodgers, E., Wilheit, T. and Siddalingaiah, H. Preprints, Fourth Conference on Hydrometeorology. Amer. Meteor. Soc., Boston, Mass. 8 pp. (1981).

8. U. S. Department of Commerce Federal Meteorological Handbook No. 7: Weather Radar Observations. Washington, D. C., various paging (1982).

9. Wilson, J. W. and Brandes, E. A. Bull. Amer. Meteor. Soc. 60, 1048-1058 (1979).

10. Smith, E. A. IEEE Transactions on Geoscience Electronics. GE-13, 123-136 (1975).

11. Spencer, R. W., Olson, W. S., Wu, R., Martin, D. W., Weinman, J. A. and Santek, D. A. "Heavy Thunderstorms Observed over Land by the Scanning Multichannel Microwave Radiometer" Submitted to J. Appl. Meteor. (1983).

12. Wilheit, T. T., Chang, A. T. C., King, J. L., Rodgers, E. B., Nieman, R. A., Krupp, B. M., Milman, A. S., Stratigos, J. S., and Siddalingaiah, H. J. Appl. Meteor. 21, 1137-1145 (1982).

13. Hakkarinen, I. M., Rodgers, E. B., and McCumber, M. C. Preprints, Conference on Cloud Physics, Amer. Meteor. Soc., Boston, Mass. 504-507 (1982).

14. Dixon, W. J., and Brown, M. B. Biomedical Computer Programs P-Series. University of California Press, 880 pp. (1977).

## Figures

Fig. 1. SMMR 37 GHz vertically polarized image of the central United States at 1730 GMT 13 July, 1979 (a), and the corresponding digitized radar image (b). The range of brightnesses in (a) represent temperatures from 229 to 290 K. The range of brightnesses in (b) represents rain rates from zero (light grey) to 45 mm/hr (white).

Fig. 2. A composited radar image comprised of all the rain systems used in the algorithm development. The range of brightnesses represent rain rates from zero (light grey) to 80 mm $hr^{-1}$ (white).

Fig. 3. A scatter plot of the radar-measured rain rates vs. the microwave algorithm-derived rain rates for the dependent (training) data set. This set is comprised of 3813 data points representing colocated radar and microwave data, each averaged over 1600 $km^2$ areas. Sample error bars are shown for the rain rates, as well as a line of slope 1, which is also a least-squares fit.

Fig. 4. A scatter plot of the radar vs. microwave measured rain rates for the independent algorithm test, with a line of slope 1. Sample error bars are shown for the radar rain rates. The wide shaded area at the origin contains approximately 100 points while the small shaded area contains 270. The inset shows a frequency histogram of the predicted rain rates for radar rain rates of zero, in intervals of 0.15 mm/hr.

7/RS1/12

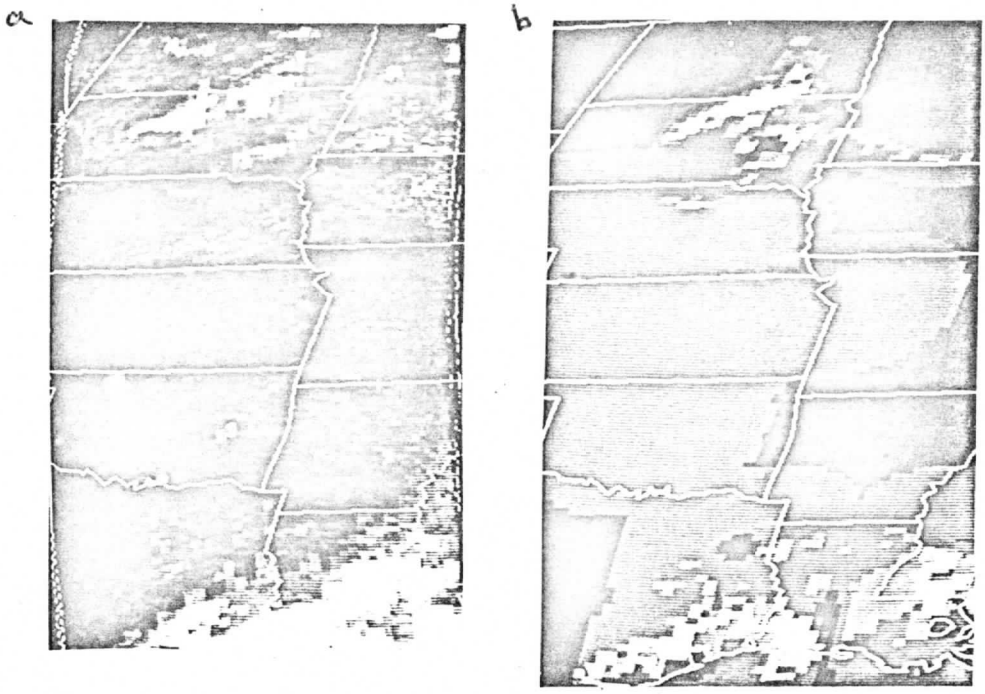


Fig. 1

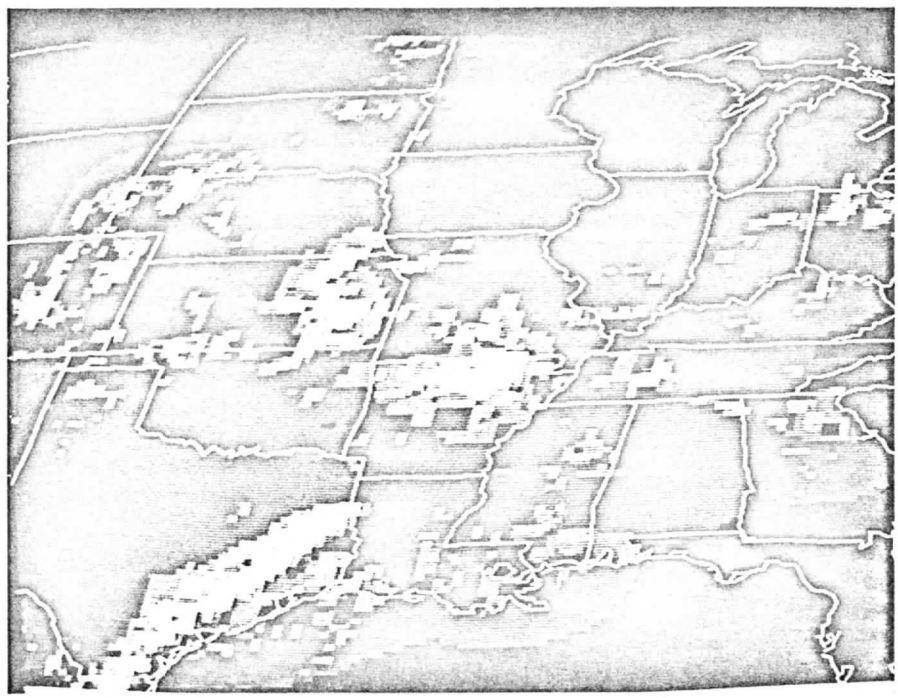

Fig. 2

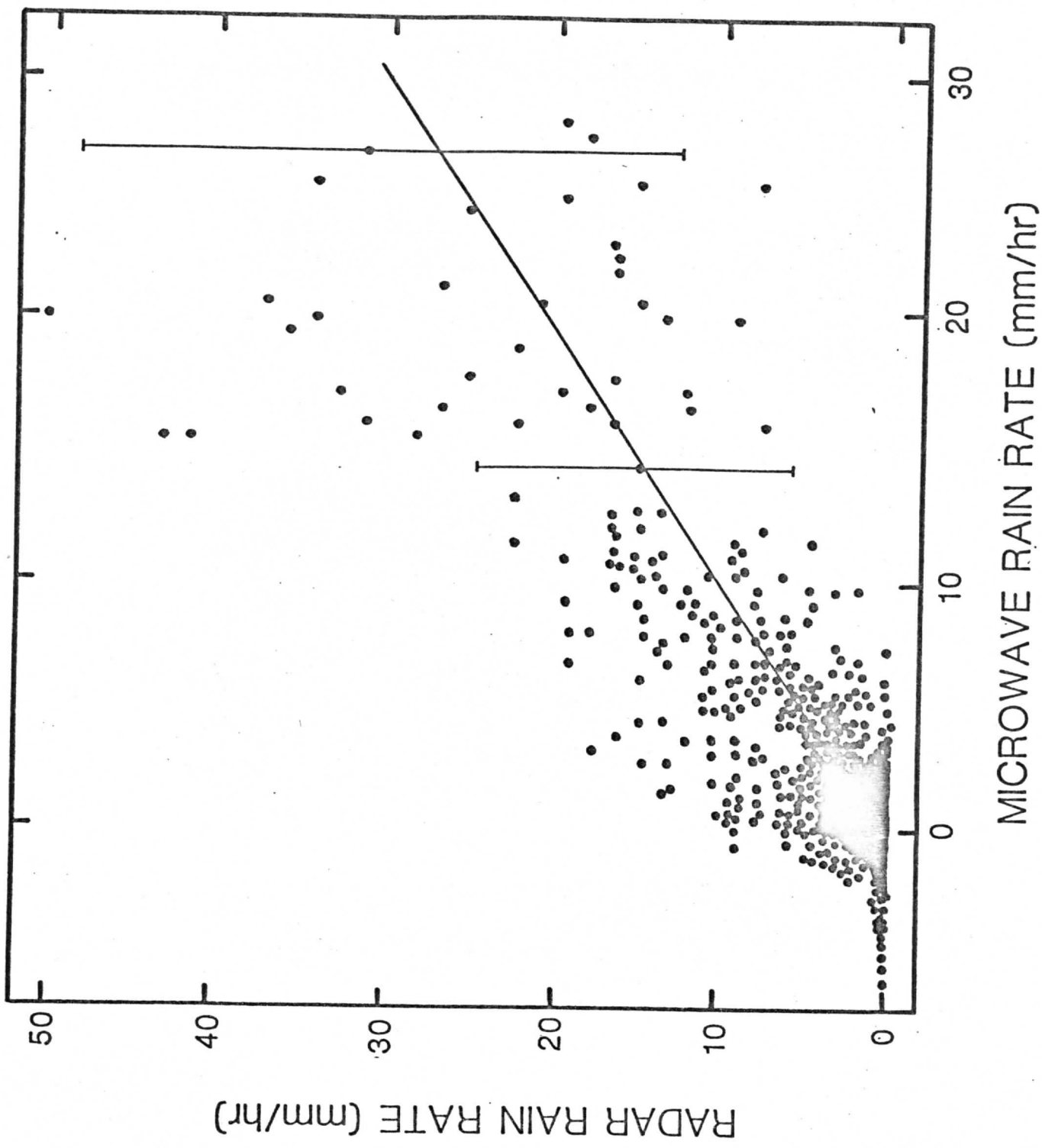
RADAR RAIN RATE (mm/hr)
0
10
20
30
40
50
MICROWAVE RAIN RATE (mm/hr)
0
10
20
30

Fig. 3

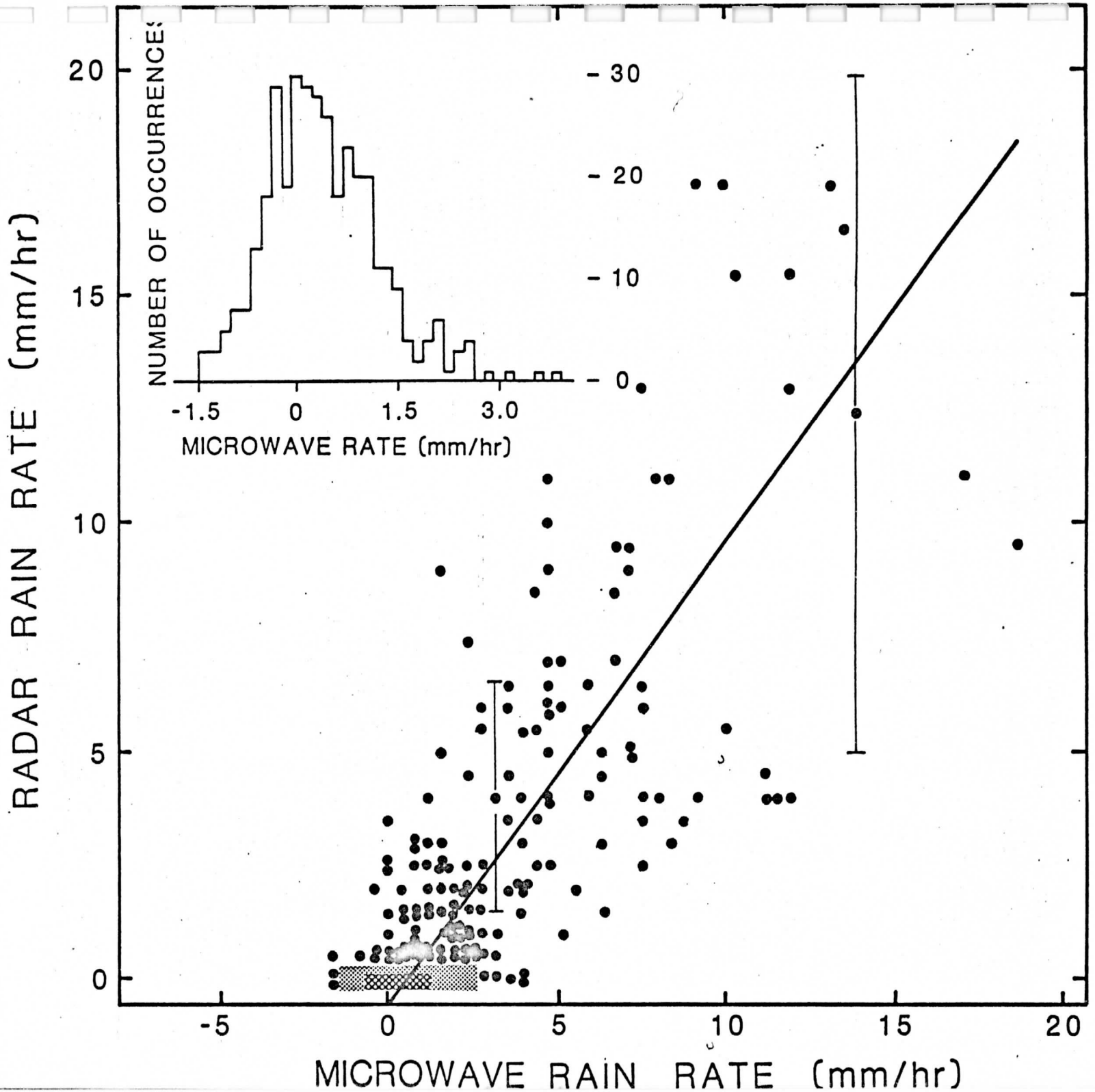
RADAR RAIN RATE (mm/hr)
MICROWAVE RAIN RATE (mm/hr)
NUMBER OF OCCURRENCES
MICROWAVE RATE (mm/hr)
20
15
10
5
0
-5
0
5
10
15
20
30
20
10
0
-1.5
0
1.5
3.0

Fig. 4

# Heavy Thunderstorms Observed Over Land by the Nimbus-7 Scanning Multichannel Microwave Radiometer

R. W. SPENCER[1], W. S. OLSON[2], WU RONGZHANG[1,2,3], D. W. MARTIN[1], J. A. WEINMAN[1,2] AND D. A. SANTEK[1]

[1] *Space Science and Engineering Center, University of Wisconsin–Madison*
[2] *Department of Meteorology, University of Wisconsin–Madison*
[3] *Central Meteorological Bureau, Beijing, People's Republic of China*

(Manuscript received 16 December 1982, in final form 17 February 1983)

ABSTRACT

In an examination of microwave data from the Nimbus 7 satellite, brightness temperatures were found that were much lower than those expected for the radiation emanating from rain-producing clouds. Every case of very cold brightness temperature coincided with heavy thunderstorm rainfall. The cold temperatures can be attributed to scattering by a layer of ice hydrometeors in the upper parts of the storms. Thus it appears that brightness temperatures observed by satellite microwave radiometers can at times distinguish heavy rain over land.

## 1. Introduction

In 37 GHz (0.8 cm) observations from the Nimbus 7 Scanning Multichannel Microwave Radiometer (SMMR; Gloersen and Hardis, 1978) an unusually low brightness temperature of 163 K was observed on 9 July 1979 over southeast Kansas. This observation contrasts with the modeled transfer of 37 GHz radiation through rain clouds, which has shown that scattering and absorption of upwelling radiation from land by rain lowers brightness temperatures to an asymptotic limit of about 230 K (Gorelik *et al.*, 1974; Savage and Weinman, 1975). So far as is known to the present authors there have been no previous reports of such a cold temperature in 37 GHz satellite observations over land. Understanding the radiative processes that produced the low brightness temperatures depends both upon an analysis of the event and a reconsideration, in light of the analysis, of models of microwave radiative transfer within rainclouds.

## 2. SMMR, infrared, and radar observations

### *a. The Kansas case*

At the time of the Nimbus 7 overpass and at the location of the very cold microwave brightness temperature, a thunderstorm was simultaneously observed by the SMS II geostationary satellite (GOES-East) and at least two National Weather Service (NWS) WSR-57 radars.

The very cold 37 GHz footprint observed in Kansas was part of a larger cold feature (Fig. 1), and it coincided with depressed brightness temperatures at 18 GHz (minimum of 239 K, Fig. 2); thus a malfunction of the instrument could be ruled out. The low brightness temperatures might be attributed to water bodies with low emissivities; however, there is no lake of dimensions comparable to those of the cold footprint in southeast Kansas. While low brightness temperature might be a consequence of widespread transient flooding, microwave radiation from water and wet surfaces is highly polarized (Rodgers, 1981; Wang and Choudhury, 1981), having up to a 60°C difference between the horizontal and vertical polarizations of the 37 GHz data. The feature observed here was only slightly more polarized (11°C) than a dry land background (8°C). The 3°C residual polarization observed above that of the nearby dry land may be due to scattering by precipitation particles (Weinman and Guetter, 1977).

The GOES-East infrared (IR) image taken within 1 min of the SMMR observation (Fig. 3) reveals a broad cirrus shield. Coldest temperatures are colocated with the lowest SMMR temperatures. The region of cold temperatures observed by the SMMR is considerably smaller than the cirrus shield; this would be expected if the SMMR was responding to hydrometeors of precipitation size within the cloud. If the Topeka KA sounding made 6 h earlier represents the ambient air temperature and if the cloud droplets are black and in radiative equilibrium with the atmosphere (see Hasler, 1981), then the coldest IR temperature, 210 K, corresponds to a height of roughly 16 km. The cirrus shield doubled its size between 0600 and 0700 (all times GMT). By 0700 it covered

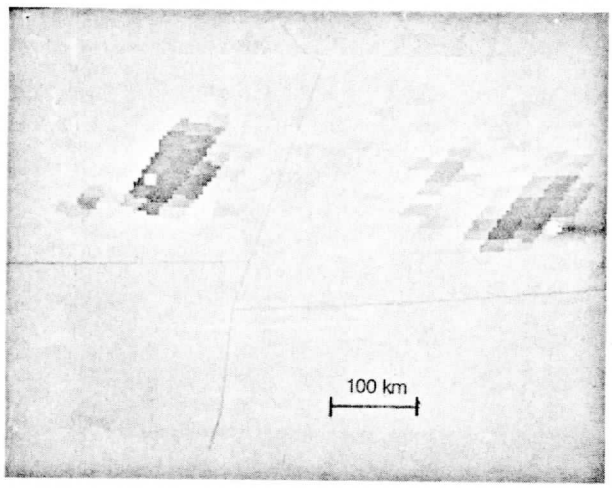


FIG. 1. SMMR 37 GHz vertically polarized brightness temperature image over the southeast Kansas area at 0635 GMT 9 July 1979, remapped to a GOES-East projection. The darkest (coldest) footprint has a horizontally polarized temperature of 163 K and a vertically polarized temperature of 174 K. Only the vertically polarized image is shown because the horizontally polarized temperatures have a one-quarter footprint line-to-line offset. The cursor shows the location of Yates Center.

the southeast one-quarter of Kansas, indicating that this storm was growing rapidly.

The NWS national radar summary for 0635 GMT indicated an east–west broken line of thunderstorms across southern Missouri and southeast Kansas moving southward. The Kansas storm was examined more closely in photographs of the Wichita KA and Monett MO radar plan position indicators (PPI's). Wichita reported a top at 18.6 km and Monett reported a top at 18.0 km, both at 0635. These heights are in general agreement with the IR-inferred height of 16 km. Both tops were located within 10 km of the very cold SMMR footprint.

Photographed reflectivities $z$ from the 0635 Monett radar PPI were converted to rainfall rates (NOAA, 1979a). Rain rates then were averaged over 20 km × 20 km bins and remapped to a GOES-East projection (Fig. 4). The possible sources of errors in this conversion are numerous: diffiering $Z$-$R$ relationships between, and even within, storms; radar beam height changes with distance from the transmitter; and video integrator and processor-level ambiguities in the PPI photographs. These factors could easily produce errors in the measured rain rates that exceed 50%. Even with these possible errors, a comparison of Fig. 4 with Fig. 1 reveals a close correspondence—in size as well as shape and orientation—between the feature seen by radar and the feature seen by satellite microwave radiometer.

Of all the storms viewed by the Monett radar at this time, only with the Kansas storm were there reports of severe weather (NOAA, 1979b). The Yates Center News documented the arrival of the storm at Yates Center (see Fig. 1) at 0620 GMT, accompanied by windspeeds in excess of 40 m $s^{-1}$ and a rainfall total of 57 mm. Hailstones caused scattered wheat crop damage, as determined from hail insurance claims. Taking these reports together, it can be said that the very cold brightness temperature coincided with an intense thunderstorm.

### *b. Other cases*

A cold area over southeast Missouri is also prominent in Fig. 1. As in the Kansas case, it closely matches a rain area depicted by the radar (Fig. 4). The lowest microwave temperature is 199 K; the

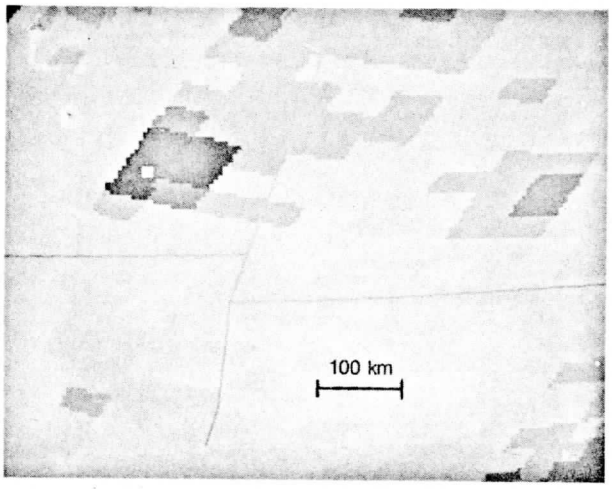


FIG. 2. As for Fig. 1, except 18 GHz. The darkest footprint has a temperature of 239 K. The lower spatial resolution and radiative transfer characteristics associated with the 18 GHz channel makes it less responsive to the precipitation within the storm, and results in a much higher temperature than that measured by the 37 GHz sensor.

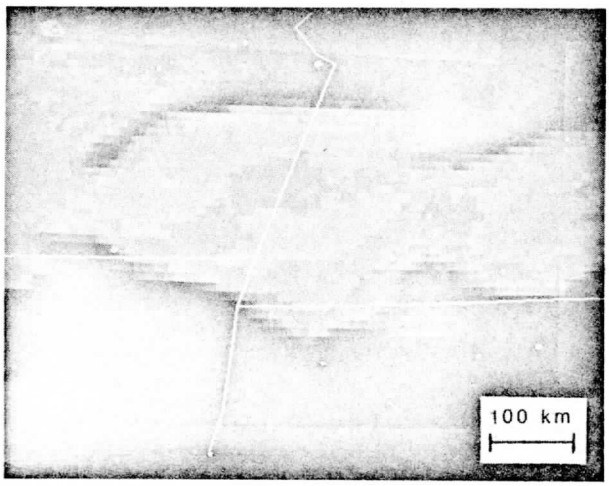


FIG. 3. SMS-II IR image for 0635 GMT 9 July 1979 over the same area as in Fig. 1.

highest rain rate, averaged over 20 km bins, is 36 mm $h^{-1}$. No severe weather was reported for this storm (NOAA, 1979b). Other cold centers in Fig. 1 also are associated with heavy rain. In these systems the lowering of the central temperature with respect to the background levels is roughly proportional to the rain rates. These observations suggest that very cold SMMR temperatures coincide with very heavy rain rates.

To test this hypothesis, the NWS radar summary charts were scanned for May–July 1979 at the times of SMMR overpasses (twice per day, every other day). Ten times were chosen that had the highest radar reflectivities and/or the tallest echoes. Comparing radar to satellite there was close agreement (to within a SMMR footprint) between the highest and strongest echoes observed by radar and the locations of the SMMR footprints with temperatures less than 210 K.

The case which had the coldest SMMR brightness temperatures occurred on 4 May 1979 in conjunction with a squall line near the Texas Gulf coastline (Fig. 5). Within this line, nine individual storms had 37 GHz brightness temperatures that ranged from 180 to 207 K. As in the Kansas case, these cold spots were only slightly more polarized (11°C) than the dry land background (8°C). Brightness temperatures at 18 GHz (not shown) were also depressed. Radar reflectivities of PPI photographs from four radars were digitized (Fig. 6) and a close correspondence was found between the lowest temperatures and the highest rain rates. A scatter plot of this relationship (Fig. 7) reveals that 37 GHz observations of heavy thunderstorms provide information on a wide range of rain rates. Considering that some of the scatter can be attributed to errors associated with the radar observations, discussed earlier, it appears that there is a relationship between cold brightness temperature and heavy rain rates.

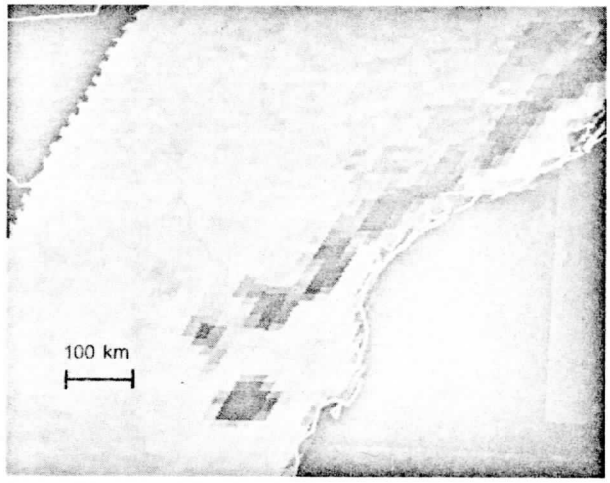


FIG. 5. SMMR 37 GHz vertically polarized brightness temperature image over Texas at 0648 GMT 4 May 1979 remapped to a GOES-East projection. The darkest (coldest) footprints have horizontally and vertically polarized brightness temperatures in the range 180–200 K and 191–211 K, respectively.

## 3. Model calculations of brightness temperature

Most efforts to model microwave brightness temperatures have assumed a rain layer extending upward to the freezing level, above which ice crystals were neglected because of their near transparency at the frequncies of interest. It might be argued that the models should allow liquid water above the freezing level. However, even in the most extreme cases of rapid ascent in updrafts, liquid water exists only to

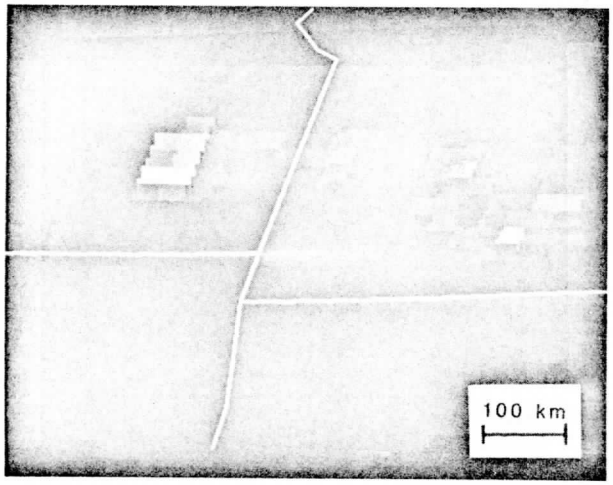


FIG. 4. Rain rates from the Monett, MO radar in 20 km × 20 km bins displayed as brightnesses and remapped to a GOES-East projection. The brightest image element in southeast Kansas corresponds to a rain rate of 65 mm $h^{-1}$.

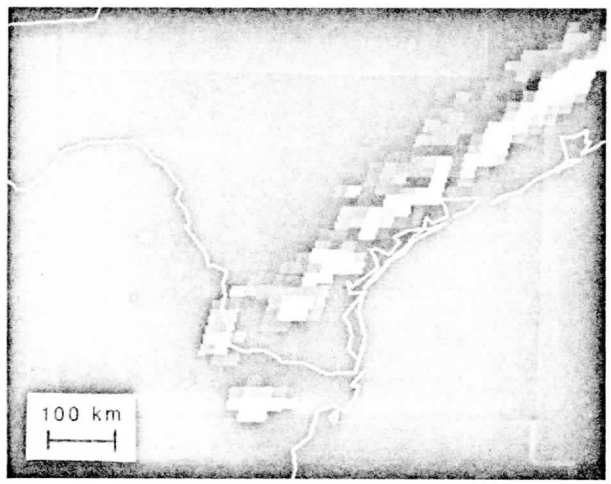


FIG. 6. Digitized rain rates from the Brownsville, Hondo and Galveston, Texas and Lake Charles, Louisiana radars at 0648 GMT 4 May 1979. See Fig. 4 for details. Rates shown are for range 6–88 mm $h^{-1}$.

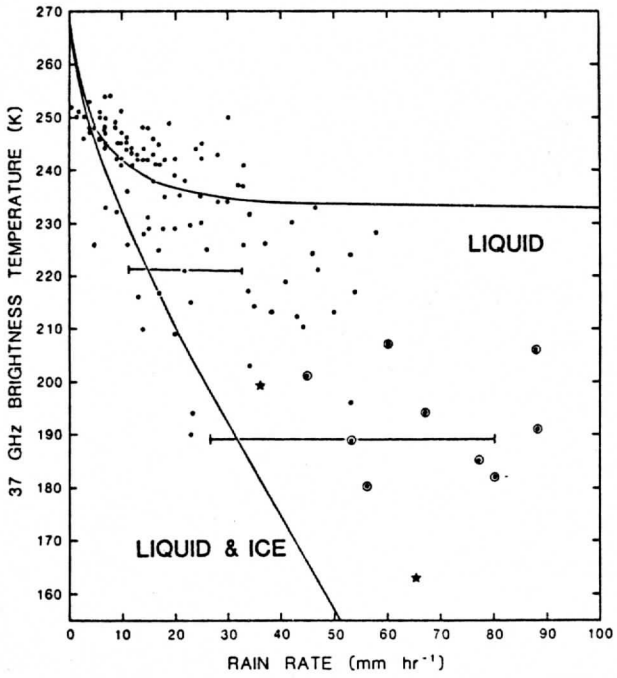


FIG. 7. Radar-derived rain rates as a function of observed 37 GHz horizontally polarized brightness temperatures for storms in Kansas and Missouri (0635 GMT 9 July 1979) and Texas (0648 GMT 4 May 1979). Dots represent all rain areas within the Texas squall line, data from which were sampled within adjacent 17 km × 17 km boxes. Circled dots represent the coldest temperatures within individual storms. The two stars represent the coldest temperatures associated with the Kansas and Missouri storms. Sample error bars of 50% in rain rate are shown for two points. No-rain cases were in the 255–270 K range. Also shown are the relationships derived from a radiative transfer model of liquid precipitation (upper curve) and a model that considers liquid and ice hydrometeors (lower curve).

a temperature of about 233 K (Ludlam, 1980, p. 209). That temperature for the Kansas case corresponds to a height of about 10 km. Savage's (1976) computations suggest that rain layers over land which extend to this altitude produce brightness temperatures no lower than ~210 K. Therefore, liquid precipitation alone cannot explain the measured brightness temperature of 163 K shown in Fig. 1.

Savage (1976) calculated brightness temperatures of clouds containing ice precipitation characterized by a Marshall and Palmer (1948) size distribution extending upward to 7 km. He found that much lower temperatures might be expected from optically thick ice clouds; however, these results were largely ignored in the literature. Weinman and Davies (1978) and Wilheit *et al.* (1982) have also modeled the effects of ice precipitation and these results also provided brightness temperatures less than those expected from liquid rain clouds.

To remedy the most obvious deficiency of earlier models, calculations have been made with a model that includes an ice layer over liquid water. A radiative transfer model based on the Neumann solution of Weinman and Guetter (1977) was used to compute the brightness temperatures that would be measured at 37 GHz at a zenith angle of 50°. The radiative properties of the hydrometers were derived from Mie theory. The refractive indices of water and ice were obtained from the review of Ray (1972). Height profiles of temperature and, indirectly, the concentration of molecular oxygen were obtained from the Topeka sounding of 00 GMT 9 July 1979. This sounding was approximately 10°C warmer than the standard atmosphere below the tropopause. The water vapor profile was that of the standard atmosphere. Absorption of microwave radiation by oxygen and water vapor was prescribed from the models of Rosenkranz (1975) and Staelin (1966), respectively. The effects of non-precipitating liquid water are relatively small, especially in clouds where the rainfall rate exceeds 10 mm $h^{-1}$ (Olson, 1983). Non-precipitating cloud droplets are, therefore, not included in the model.

The earth's surface is characterized by a temperature of 298 K and a dry soil emissivity equal to 0.9, independent of zenith angle. Although the emissivity can be lowered significantly due to the influence of standing water or wet soil, microwave brightness temperatures are sensitive to changes in surface emissivity at rainfall rates > ~8 mm $h^{-1}$ at 37 GHz and ~20 mm $h^{-1}$ at 18 GHz, so that neither the value nor the constancy of the ground emissivity has a great bearing on the general results to follow.

Fig. 8 shows the distribution of precipitating water used in the present model. Liquid precipitation is confined to a layer between the surface and 7 km, while ice precipitation occupies a layer between 7 km and the top of the cloud. The size distributions are identified by the equivalent rainfall rate $R$ in the Marshall-Palmer (1948) formula. The variability of water content with height was assumed to follow profiles similar to that given by Geotis (1971) for the average of eight heavy thunderstorms. The water content profiles in the model are constant up to a height of 7 km, then decrease to zero at heights consistent with the radar derived height-rain rate relationships of Donaldson (1958, corrected in 1961). These profiles are in approximate agreement with the modeled results of Kessler (1982, p. 470).

It should be noted that the radiative transfer model employs simplistic assumptions regarding many of the parameters that describe the precipitation. The hydrometers are probably not distributed with altitude either in size or in number density as the model assumes. It is doubtful that the hydrometers above 7 km are all ice, or that all of the ice hydrometers, regardless of size, radiate at a temperature which is given by a nearby sounding. The model ignores these ambiguities in an attempt to provide the simplest explanation for the observed 37 and 18 GHz brightness temperatures which is consistent with the avail-

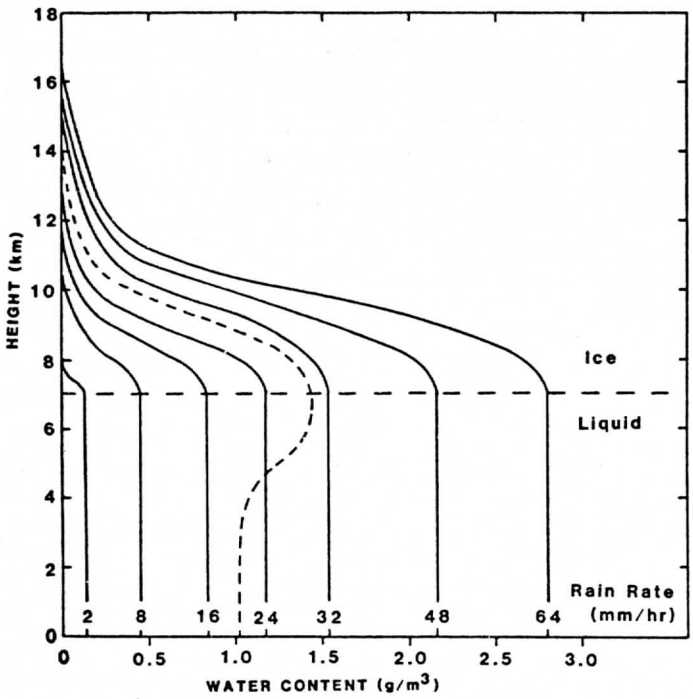


FIG. 8. Seven profiles of water content for which the radiative transfer of 37 GHz radiation was modeled. The dashed line is the average water content profile of eight heavy thunderstorms computed from radar reflectivities by Geotis (1971).

able information. A more comprehensive study that includes these effects is in progress.

The modeled 37 GHz brightness temperatures corresponding to the seven profiles in Fig. 8 yield the lower curve shown in Fig. 7. It can be seen that the inclusion of ice in the model yields much lower brightness temperatures than those resulting from the same model with no ice above 7 km (the upper curve in Fig. 7).

At higher rain rates most of the observed data fall between the two curves. The most plausible reason for this is that the SMMR field of view is rarely filled with ice. In addition, the 37 GHz footprints are larger than the nominal footprint dimensions (28 km × 21 km) suggest, so that adjacent footprints actually overlap. Thus, the rain rates corresponding to given brightness temperatures should be averaged over areas larger than 20 km × 20 km, which would lead to a more downward-sloping trend of the observed data in Fig. 7.

The radiative transfer model was also used to compute 18 GHz brightness temperatures and these were compared to the modeled 37 GHz temperatures (Fig. 9). Observations of the coldest 37 and 18 GHz brightness temperatures associated with all of the individual storms in Kansas, Missouri and Texas are plotted in Fig. 9. The modeled and measured 37 and 18 GHz brightness temperatures which are shown indicate rough agreement between the simple theory and the observations. Because the 18 GHz footprint is about four times larger than the 37 GHz footprint, the contribution by the adjacent warm land background within the footprint may raise the resultant brightness temperature to a value greater than that expected from a "rain-filled" footprint. Thus the 18 GHz brightness temperatures measured by SMMR that are shown in Fig. 9 are biased toward higher values compared to the 37 GHz temperatures. It may be inferred from Fig. 9 that the 18 GHz radiances are less sensitive to changes in rain intensity than the 37 GHz radiances. The modeled 18 and 37 GHz temperatures suggest, however, that rain rates considerably in excess of 20 mm $h^{-1}$ were present. This agrees with the measured results shown in Fig. 7.

## 4. Conclusions and implications

Measurement of intense rainfall rates over land by means of satellite-borne passive microwave radiometers has generally been regarded as a difficult task (see Atlas and Thiele, 1981). Earlier radiative transfer models and some limited observations of storms have suggested that microwave brightness temperatures measured over land at 37 GHz become insensitive to rainfall at rates greater than about 20 mm $h^{-1}$. However, it has been shown here that even over land brightness temperatures much colder than those predicted from rain layer models occasionally are ob-

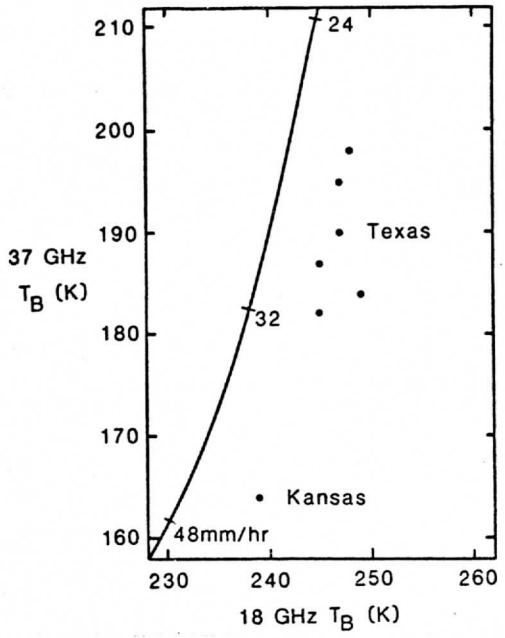


FIG. 9. Modeled (curve) and observed (dots) relationship between the 37 and 18 GHz brightness temperatures at given rain rates. The observed brightness temperatures are horizontally polarized; however, the modeled temperatures are unpolarized when the rain is optically dense.

served and that in every case of cold brightness temperature heavy rain was observed at the surface. The cold temperatures can be explained if there is a thick layer of precipitation-sized ice hydrometeors above the rain. The same structure—presumably a wide, strong updraft—that allows a storm to carry precipitation well above the freezing level apparently also favors heavy rain. Thus it appears that the 37 GHz observations do at times contain information on relatively heavy rain rates. The coincidence of the coldest brightness temperatures with the most extreme weather events suggests as well that the 37 GHz channel may have some value in detecting severe local storms. Additional theoretical work is needed to determine how sensitive model results are to drop size distributions, particularly those of ice, to ice hydrometeors wetted with water, and to the size of the rain cell. More definitive radar and *in situ* observations would help to establish the validity of the analysis.

*Acknowledgments.* Funding for this study was provided by the National Oceanic and Atmospheric Administration National Earth Satellite Service through Grant NA-80-SAC-00742 and the National Aeronautics and Space Administration through Grant NAGW-380. SMMR data were provided by Per Gloersen and William Abbott of the Goddard Space Flight Center; their cooperation is appreciated. The manuscript was typed by Angela Crowell and Jody Edwards.

## REFERENCES

Atlas, D., and O. W. Thiele, 1981: Precipitation measurements from space. Workshop report, Goddard Space Flight Center, $$ pp. So pp plus appendices.

Donaldson, R. J., Jr., 1958: Analysis of severe convective storms observed by radar. *J. Meteor.*, **15**, 44–50.

——, 1961: Radar reflectivity profiles in thunderstorms. *J. Appl. Meteor.*, **18**, 292–305.

Geotis, S. G., 1971: Thunderstorm water contents and rain fluxes deduced from radar. *J. Appl. Meteor.*, **10**, 1233–1237.

Gloersen, P., and L. Hardis, 1978: *The Nimbus 7 Users' Guide.* National Aeronautics and Space Administration, 213–245.

Gorelik, A. G., V. V. Kalashnikov and Y. A. Frolov, 1974: Possibility of precipitation zone identification from meteorological satellites. *Advances in Satellite Meteorology,* Vol. 2, N. K. Vinnichenko and A. G. Gorelik, Eds., Wiley, 148 pp.

Hasler, A. F., 1981: Stereographic observations from geosynchronous satellites: An important new tool for the atmospheric sciences. *Bull. Amer. Meteor. Soc.*, **62**, 194–212.

Kessler, E. K., 1982: *Thunderstorm Morphology and Dynamics.* National Oceanic and Atmospheric Administration, 603 pp.

Ludlam, F. H., 1980: *Clouds and Storms.* The Pennsylvania State University Press, 396 pp.

Marshall, J. S., and W. Mck. Palmer, 1948: The distribution of raindrops with size. *J. Meteor.*, **5**, 165–166.

NOAA, 1979a: *Introduction to Weather Radar.* U.S. Department of Commerce, 70 pp.

——, 1979b: *Storm Data,* **21.** U.S. Department of Commerce, 25 pp.

Olson, W. S., 1983: Estimation of rainfall rates in tropical cyclones by passive microwave radiometry. Ph.D. thesis, University of Wisconsin, Madison, $$$ pp.

Ray, P. S., 1972: Broadband complex refractive indices of ice and water. *Appl. Opt.*, **11**, 1836–1843.

Rodgers, E., 1981: The utilization of satellite passive microwave sensors to monitor synoptic scale rainfall. *Precipitation Measurements from Space,* Workshop report, Goddard Space Flight Center, $$$–$$$. Appen. D, 234-245.

Rosenkranz, P. W., 1975: Shape of the 5 mm oxygen band in the atmosphere. *IEEE Trans. Antennas Propagat.*, **AP-23**, 498–506.

Savage, R. C., and J. A. Weinman, 1975: Preliminary calculations of the upwelling radiance from rainclouds at 37.0 and 19.35 GHz. *Bull. Amer. Meteor. Soc.*, **56**, 1272–1274.

——, 1976: The transfer of thermal microwaves through hydrometeors. Ph.D. thesis, University of Wisconsin, Madison, 147 pp.

Staelin, D. H., 1966: Measurements and interpretation of the microwave spectrum of the terrestrial atmosphere near 1-cm wavelength. *J. Geophys. Res.*, **71**, 2875–2881.

Wang, J. R., and B. J. Choudhury, 1981: Remote sensing of soil moisture content over bare fields at 1.4 GHz frequency. *J. Geophys. Res.*, **86**, 5277–5282.

Weinman, J. A., and R. Davies, 1978: Thermal microwave radiances from horizontally finite clouds of hydrometeors. *J. Geophys. Res.*, **83**, 3099–3107.

——, and P. J. Guetter, 1977: Determination of rainfall distributions from microwave radiation measured by the Nimbus-6 ESMR. *J. Appl. Meteor.*, **16**, 437–442.

Wilheit, T. T., A. T. C. Chang, J. L. King, E. B. Rodgers, R. A. Nieman, B. M. Krupp, A. S. Milman, J. S. Stratigos and H. Siddalingaiah, 1982: Microwave radiometric observations near 19.35, 92, and 183 GHz of precipitation in Tropical Storm Cora. *J. Appl. Meteor.*, **21**, 1137–1145.

APPENDIX 4

# Nimbus-7 37 GHz Radiances Correlated with Radar Rain Rates over the Gulf of Mexico

by

Roy W. Spencer,[1] Barry B. Hinton,[1] and William S. Olson[2]

[1]Space Science and Engineering Center and
[2]Department of Meteorology
University of Wisconsin-Madison
Madison, Wisconsin 53706

Submitted to
Journal of Climatology and Applied Meteorology

June 1983

## Abstract

In a comparison between 37 GHz brightness temperatures from the Nimbus 7 Scanning Multichannel Microwave Radiometer and rain rates derived from the WSR-57 radars at Galveston, Texas and Apalachicola, Florida, it was found that the brightness temperatures explained 72% of the variance of the rain rates. The functional form relating these two types of data was significantly different from that predicted by models of radiative transfer through plane-parallel clouds. Most of the difference can be explained in terms of the partial coverage of footprints by convective showers. Because residual polarization is always present, even for large obscuring storms over land and water, it is hypothesized that emission by non-spherical rain drops is at least partly responsible for the observed polarization.

## 1. Introduction

The transfer of 37 GHz microwave radiation through rain over the ocean has usually been modeled with horizontally infinite clouds of spherical hydrometeors (e.g., Savage, 1976; Weinman and Guetter, 1977; Rodgers et al., 1979; Olson, 1983; Huang and Liou, 1983). Typically, the results of these experiments show that the emission from rain raises the observed brightness temperature above that of the ocean surface, which appears relatively cold because of its low emissivity, until the rain rate reaches 5 to 10 mm $h^{-1}$. The brightness temperature decreases gradually at higher rain rates to an asymptotic limit for rain rates greater than about 20 mm $h^{-1}$. This decrease above 5-8 mm $h^{-1}$ is partly due to scattering of upwelling radiation, as well as emission at lower temperatures. As the rain cloud becomes more dense at higher rain rates, the radiative emission seen by a downward looking radiometer originates from increasingly higher (colder) levels.

Over the tropics and warmer regions, however, the $\sim$500 $km^2$ footprint of the 37 GHz channel of the Nimbus 7 Scanning Multichannel Microwave Radiometer (SMMR, Gloersen and Hardis, 1978) is probably seldom filled with rain (except occasionally in the special case of tropical cyclones). This is because of the relatively small size of individual showers and the multicellular nature of shower complexes. This effect had been observed during the GATE (GARP Atlantic Tropical Experiment) when the Nimbus 5 ESMR (Electrically Scanning Microwave Radiometer), a 19.35 GHz instrument, was used to estimate rainfall and the results were compared to radar measurements (Medrow, et al., 1982; Austin and Geotis, 1978; Smith and Kidder, 1978). It was found that the

satellite underestimated the rain rates by 40% to 50% when compared to the radar estimates. It was also found that the microwave sensor footprint filling estimated by radar could not alone account for the differences between the radar and satellite measurements.

We present observations that reveal the departures of observed 37 GHz radiation from plane parallel theory for warm season showers over the Gulf of Mexico, and discuss some possible explanations for the observed discrepancies.

## 2. SMMR and Radar Observations

Coincident radar and SMMR 37 GHz observations were analyzed over the Gulf of Mexico within the 230 km radius scans of the WSR-57 radars operated by the U.S. National Weather Service (NWS) at Galveston, Texas on five days and at Apalachicola, Florida on one day (Table 1). Reflectivities from radar Plan Position Indicator (PPI) microfilm records were manually digitized on a 20 km grid and converted to average rain rates for each 20 x 20 km bin (see Spencer et al., 1983a). The errors in these radar measurements of rain rate are numerous. They include differing reflectivity-rain rate relationships between and even within storms, calibration changes, radar beam height change with distance from the transmitter, attenuation of the radar beam by heavy rain, evaporation of rain, rain traveling with the wind before reaching the earth, and false echoes due to anomalous propagation. Nevertheless, the radars and SMMR have similar temporal and spatial sampling characteristics; i.e., they both observe instantaneously over spatially continuous areas.

| Radar | Date | SMMR Observation Time (GMT) | Radar Observation Time (GMT) |
|---|---|---|---|
| Galveston, TX | 16 April, 1979 | 1801 | 1801 |
| Galveston, TX | 27 June, 1979 | 1755 | 1756 |
| Galveston, TX | 7 July, 1979 | 1735 | 1734 |
| Galveston, TX | 9 July, 1979 | 0638 | 0639 |
| Galveston, TX | 13 July, 1979 | 1744 | 1745 |
| Apalachicola, FL | 17 July, 1979 | 0530 | 0538 |

Table 1. Dates and times of SMMR and radar data used in this study.

Data from approximately thirty-five storms were included. Images were generated from both the digitized rain rates and the SMMR observations on the University of Wisconsin-Madison Man-computer Interactive Data Access System (McIDAS, Smith,1975). The SMMR images were adjusted for navigation errors using the brightness temperature contrast of land-water boundaries. These errors were always less than 20 km, and after correction are within 5 km. The radar and SMMR images were sampled on a 20 km grid and geographically matched pairs of rain rate and brightness temperature were plotted (Fig. 1). The brightness temperatures are seen to increase as the bin averaged rain rates increase. A sixth power function of the 37 GHz brightness temperature (the curve shown in Fig. 1) has a correlation coefficient of 0.85, revealing that the SMMR horizontally polarized 37 GHz observations can account for 72% of the variance of the radar rain rates. The differences between the observed brightness temperatures and those predicted by plane-parallel theory (Olson, 1983 which assumes a rain filled sensor footprint) are marked, especially at low rain rates.

The differences between plane-parallel theory and observation are also substantial for the 37 GHz polarization (defined here as the vertical minus horizontal brightness temperature) as a function of rain rate (Fig. 2). The polarization of the radiation emanating from the ocean surface is typically 50°-60°C after modification by the intervening atmosphere, which is taken into account by the model. The model indicates that the polarization should drop to near zero if the field of view is covered with a rain layer with rate above 5 mm $h^{-1}$. These results are typical of most other investigations. A notable exception is the Huang and Liou (1983) general solution for the transfer

of thermal radiation in scattering atmospheres, including the polarization effects of Mie particles. At 37 GHz they found that scattering results in negative polarization when the rain rate exceeds 7 mm $h^{-1}$, reaching -2°C at 20 mm $h^{-1}$. The observations (also in Fig. 2) reveal much larger, positive polarizations.

We first tried to explain these differences between plane-parallel theory and observation with partial footprint filling by the showers. The same rain systems were further analyzed from the PPI photographs. The fractional coverage of each 20 km bin by rain was estimated, as well as the average rain rate for the raining portion of that bin. We used the theoretical relation between the horizontally polarized brightness temperature and rain rate to estimate the brightness temperature that should emanate from the raining portion of the bin. The non-raining portion was assigned a brightness temperature which was the value predicted by the model (166K) and that observed to be typical of rain free portions of the Gulf. These two temperatures were area averaged. The result is plotted as a function of bin-average rain rate in Fig. 3. The relationship implied by these data is somewhat closer to the observed relationship between rain rate and brightness temperature, but some large differences remain. It was found that the difference seen here is relatively independent of the Z-R relationship used to derive the rain rates from the radar reflectivities.

An additional factor resulting in the discrepancy between the observed and theoretical relationships shown in Figs. 1 and 2 is rain cell geometry. The intensity of radiation upwelling from a model rain cloud of finite horizontal extent over the ocean is typically less than that upwelling from a plane-parallel cloud with the same height and

rainfall rate. Weinman and Davies (1978) modeled rain cells with finite cloud geometry. Their results show that this effect is greatest for relatively small rain cells (less than ∿6 km diameter) or relatively light rain rates (less than ∿5 mm $h^{-1}$). The radar observations revealed that these are infrequently satisfied conditions. The average storm size was 15 km and the average storm rain rate was 15 mm $h^{-1}$, values at which the "finite cloud" effects are almost negligible.

If all the residual polarization at high rain rates was due to patches of the radiometrically cold ocean surface being in view, then the observed horizontally and vertically polarized brightness temperatures should both be lower than the theory predicts for radiation emanating from thick rain layers. This was found to not be the case for the largest storms observed. A line of large (up to 80 km diameter), intense thunderstorms observed by the Apalachicola, Florida radar had tops exceeding 14 km. Simultaneous SMMR 37 GHz observations revealed vertically polarized brightness temperatures up to 252 K (with 20°C polarization) in these storms, coincident with the heaviest rain rates which exceeded 30 mm $h^{-1}$ averaged over 400 $km^2$. Fig. 4 shows the observed 37 GHz vertically polarized brightness temperature -- rain rate relationship for the showers observed by the Apalachicola and Galveston radars, along with the relationship derived from plane-parallel theory for rain filled footprints. The observed 37 GHz brightness temperatures of the Apalachicola storms are at least 5°C warmer than the theory predicts at the highest rain rates. Corrections for the most obvious sources of errors in the model assumptions would lead to even a larger temperature difference. A more appropriate model that would include the great depth of the rain layer and the presence of ice would have

produced much lower brightness temperatures, and the discrepency between the model and observations would probably have exceeded 20°C. Spencer et al. (1983b) showed SMMR 37 GHz observations of heavy thunderstorms over land that exhibited vertically polarized brightness temperatures as low as 174 K, with 11°C polarization compared to 5°to 8°C polarization for the surrounding land. A more extensive sample of 37 GHz brightness temperatures of tropical convection scattered over a $5 \times 10^5$ $km^2$ area in the Pacific (not shown) were compared to GOES-West infrared and visible pictures. The highest brightness temperature regions corresponded to deep convective activity. Again, these rain cells had polarizations above 10°C, with vertically polarized temperatures between 255 K and 258 K. Thus, there is substantial evidence for a significant polarization of the radiation emanating from the tops of rain layers that is independent of the ocean surface contribution.

Two possible explanations for the observed polarization are scattering and emission of polarized radiation from non-spherical raindrops. Nearly all of the models of the upward transfer of passive microwave radiation through rain clouds to a downward looking radiometer, that we are aware of, contain the assumption that the raindrops are spheres that emit radiation isotropically. Huang and Liou (1983) have shown that scattering by spherical drops results in a slight negative polarization. However, raindrops, especially the larger ones, are not spheres but have a preferred flattened shape, with the short axis oriented vertically. The scattering properties of these drops have been studied extensively by communications engineers who have observed and modeled the marked differential attenuation effect these drops have on polarized microwave communication signals. A comprehensive review of

much of this work is provided by Oguchi (1981). How the scattering and emission effects combine to produce the 10°-20°C polarization that we observe with the widest and deepest (and thus most obscuring) storms we cannot say. These effects, however, should be addressed before useful quantitative rain estimates can be made from theoretically-based algorithms.

## 3. Conclusions and Implications

From the aforementioned considerations, we conclude that the footprint observed by the satellite 37 GHz radiometer is seldom covered by rain. The same statement concerning footprint filling would be even more applicable to the 18 GHz channel since its footprint is approximately four times the size of the 37 GHz footprint. Additionally, due to the radar evidence for large numbers of optically thick rain showers (greater than 5 mm $h^{-1}$), we conclude that the primary cause of variations in observed 37 GHz brightness temperatures over the ocean is footprint filling by relatively opaque showers. This contrasts with a simple application of plane-parallel theory in which the brightness temperatures vary only with the rain opacity at low rain rates (less than 5 mm $h^{-1}$). Finally, because there is always 10°-20°C polarization present with the largest storms (even over land) scattering and emission by rain probably contributes to polarization of the satellite-sensed radiation.

Observations of showers at 37 GHz over the ocean contain much the same information as the radar-derived rain rates averaged over 20 x 20 km areas for approximately 35 storms observed on six days. The relationship between brightness temperature and rain rate in this

limited group of observations is quite different than that given by plane-parallel theory. The relatively high correlation between rain rate and brightness temperature (0.85) suggests that footprint filling (and possibly other) effects are naturally correlated with footprint-averaged rain rate. Thus, it may not be necessary to invoke multispectral satellite techniques (e.g., visible and infrared; see Smith and Kidder, 1978) to estimate the footprint filling independently, unless rainfall information is sought on a spatial scale finer than that provided by the microwave sensor. Additional modeling of typical size and shape distributions of tropical showers within the radiometer field of view, and the scattering and emission characteristics of the raindrops within these showers over the ocean, should help to explain the observed brightness temperature -- rain rate relationship. We suggest that modifications of plane-parallel models are needed before they can provide accurate estimates of rain rate, particularly in regions where the radiometer's relatively large field of view is seldom filled with rain. Alternatively, an empirical algorithm based upon large numbers of SMMR and radar comparisons over coastal waters covered by these radars should provide useful estimates of oceanic rain rate. If the observed relationship (or one like it) holds up over the tropics and other showery regions, it should prove more useful than the theoretical relations until they are modified to adequately deal with beam filling, the presence of ice, the variable depth of the rain layer, and rain-induced polarization of radiation.

Acknowledgements. This work benefitted from discussions with Dr. David Martin, who did not deny the possibility of a significant rain-induced

polarization and inspired the search for its existence, and also from Professor James Weinman. Funding for this study was provided by the National Oceanic and Atmospheric Administration National Earth Satellite Service through Grant NA-80-SAC-00742. We wish to thank Per Gloersen and William Abbott of the Goddard Space Flight Center for their generous provision of SMMR data. The manuscript was typed by Angela Crowell and Jody Edwards.

## References


Austin, P.M., and S.G. Geotis, 1978: Evaluation of the quality of precipitation data from a satellite-borne radiometer. Final report under NASA Grant NSG 5024. Department of Meteorology, Massachusetts Institute of Technology, Cambridge, Massachusetts, 02139.

Gloersen, P. and L. Hardis, 1978: The Nimbus 7 Users' Guide. National Aeronautics and Space Administration, 213-245.

Huang, R. and K.-N. Liou, 1983: Polarized microwave radiation transfer in precipitating cloudy atmospheres: applications to window frequencies. J. Geophys. Res., 88, 3885-3893.

Medrow, W., E. Raschke, and E. Ruprecht, 1982: Rainfall rates derived from Nimbus-5 observations analyzed against radar rainfall. Preprint, Sumposium uber Strahlungstransportprobleme und Satellitenmessungen in der Meteorologie und der Ozeanographie, Loln, 22-26 March. Deutscher Wetterdienst, Offenbach am Main, Fed. Rep. of Germany, 71-73.

Oguchi, T., 1981: Scattering from hydrometeors: a survey. Radio Science, 16, 691-730.

Olson, W. S., 1983: Estimation of Rainfall Rates in Tropical Cyclones by Passive Microwave Radiometry. Ph. D. Thesis, Dept. of Meteorology, Univ. of Wisconsin, Madison, WI 53706, 200 pp.

Rodgers, E., H. Siddalingaigh, A. T. C. Chang, and T. Wilheit, 1979: A statistical technique for determining rainfall over land employing Nimbus 6 ESMR measurements. J. Appl. Meteor. 18, 978-991.

Savage, R. C., 1976: The Transfer of Thermal Microwaves Through Hydrometeors. Ph.D. Thesis, Dept. of Meteorology, Univ. of Wisconsin, Madison, WI 53706, 147 pp.

Smith, E. A., 1975: The McIDAS system. IEEE Transactions on Geoscience Electronics. GE-13, 123-136.

Smith, E.A., and S.Q. Kidder, 1978: A multispectral satellite approach to rainfall estimates. Department of Atmospheric Science, Colorado State University, Fort Collins, CO 80523.

Spencer, R. W., D. W. Martin, B. B. Hinton, and J. A. Weinman, 1983a: Satellite microwave radiances correlated with radar rain rates over land. Accepted for publication in Nature, 1983.

Spencer, R.W., W.S. Olson, Wu Rongzhang, D.W. Martin, J.A. Weinman, and D.A. Santek, 1983b: Heavy thunderstorms observed over land by the Nimbus-7 Scanning Multichannel Microwave Radiometer. Accepted for publication in Journal of Climatology and Applied Meteorology, 1983.

Weinman, J. A., and R. Davies, 1978: Thermal microwave radiances from horizontally finite clouds of hydrometeors. J. Geophys. Res., 83, 3099-3107.

Weinman, J. A., and P. J. Guetter, 1977: Determination of rainfall distributions from microwave radiation measured by the Nimbus-6 ESMR. J. Appl. Meteor., 16, 437-442.

## Legends

Fig. 1 Observed 37 GHz horizontally polarized brightness temperatures from the Nimbus 7 SMMR vs. radar rain rates from the Galveston radar (dots) and Apalachicola radar (stars), manually digitized and assigned to 20 x 20 km bins. The line through the data points is a least squares fit of a function proportional to the sixth power of the brightness temperatures. The upper curve depicts the theoretical results of Olson (1983) for rain filled fields of view, and is representative of the results of many other investigators. The area averaged rain rates are estimated to be accurate to ±60%.

Fig. 2 Observed 37 GHz polarization (vertical minus horizontal brightness temperatures) vs. the corresponding Galveston and Apalachicola radar rain rates. The curve in the lower left is the theoretical result of Olson (1983) for rain filled fields of view.

Fig. 3 Model 37 GHz horizontally polarized brightness temperatures estimated from the areal weighting of the brightness temperatures from Olson's model by the radar observed fractional covering of 20 x 20 km bins by rain and no rain, as a function of bin averaged rain rate. See Fig. 1 for details.

Fig. 4 Observed 37 GHz vertically polarized brightness temperatures from the Nimbus 7 SMMR and radar rain rates from the Galveston radar (dots) and Apalachicola radar (stars) manually digitized and assigned to 20 x 20 km bins. An eighth power least squares fit to the data has a correlation of 0.82. See Fig. 1 for details.

7/RS2/01.1

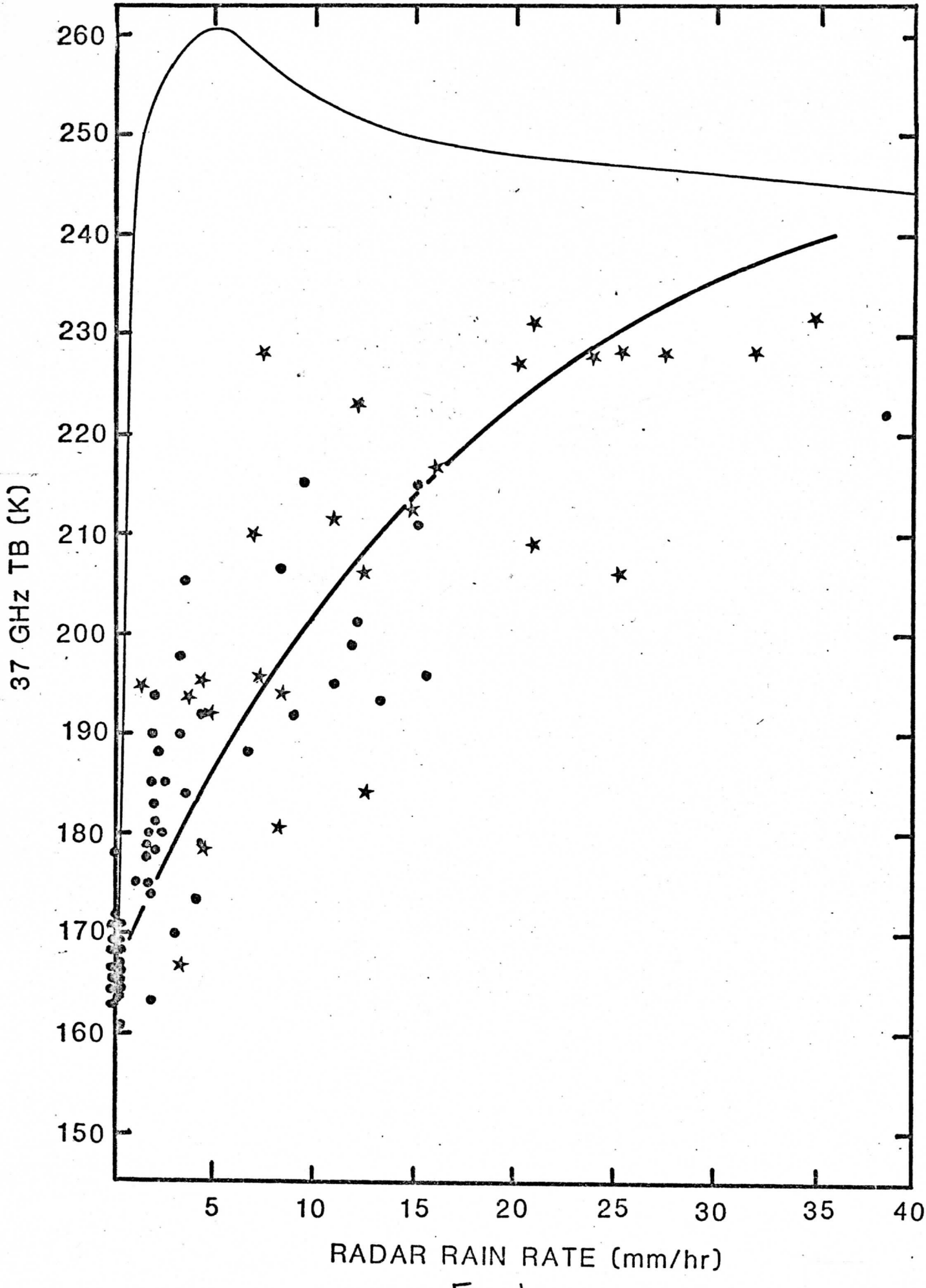
260
250
240
230
220
210
200
190
180
170
160
150
37 GHz TB (K)
5
10
15
20
25
30
35
40
RADAR RAIN RATE (mm/hr)

Fig. 1

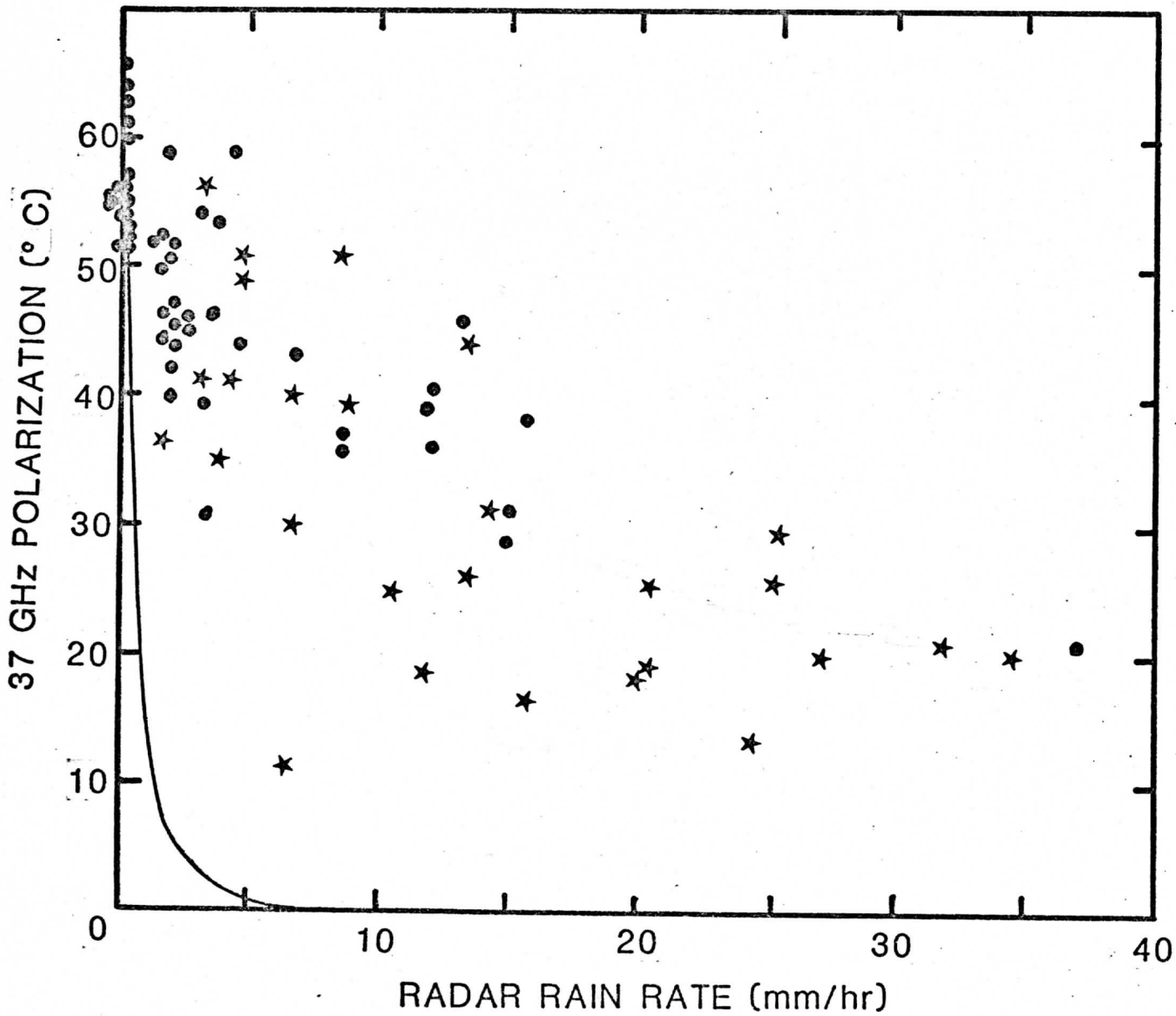
37 GHz POLARIZATION (° C)
60
50
40
30
20
10
0
10
20
30
40
RADAR RAIN RATE (mm/hr)

Fig. 2

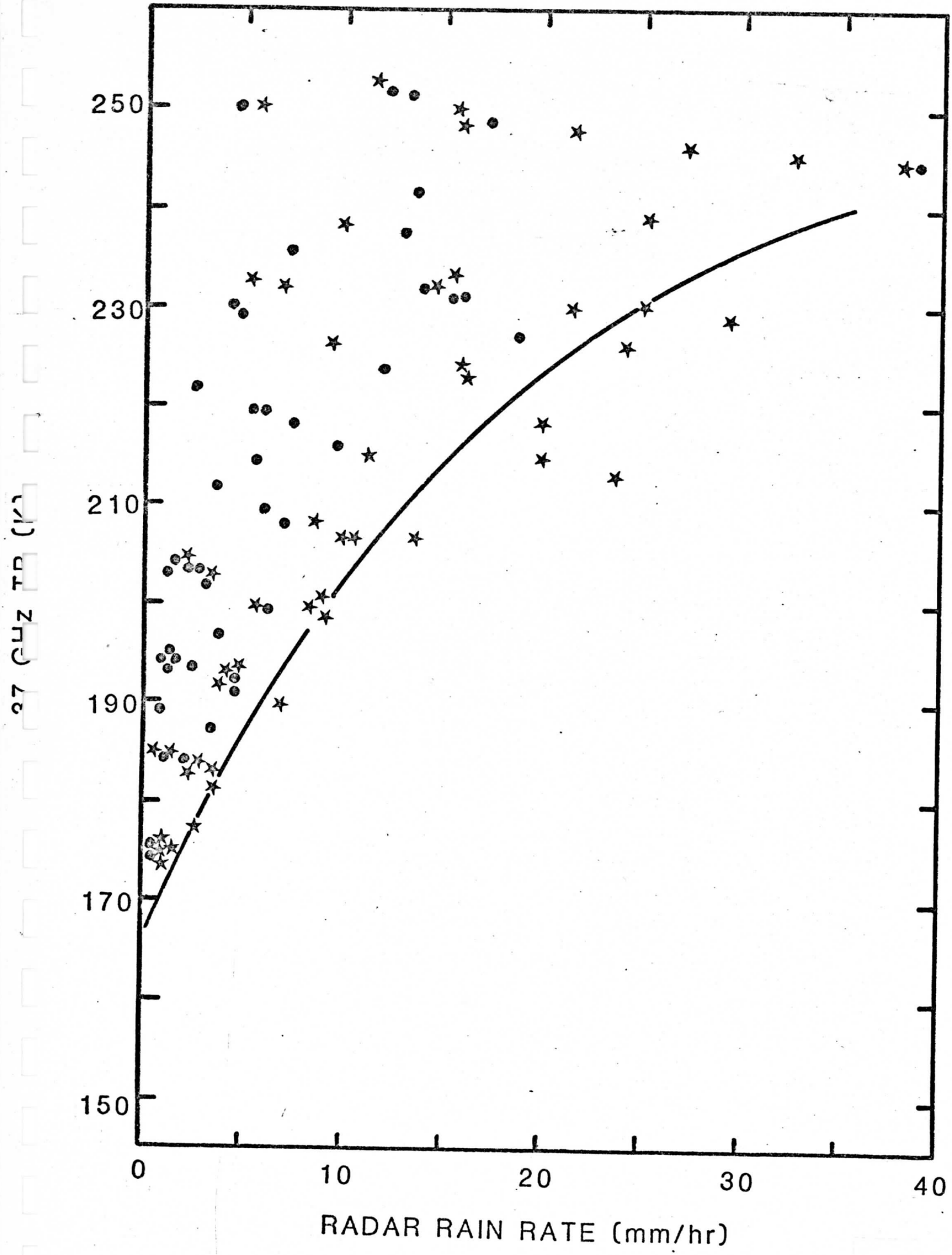


Fig. 3

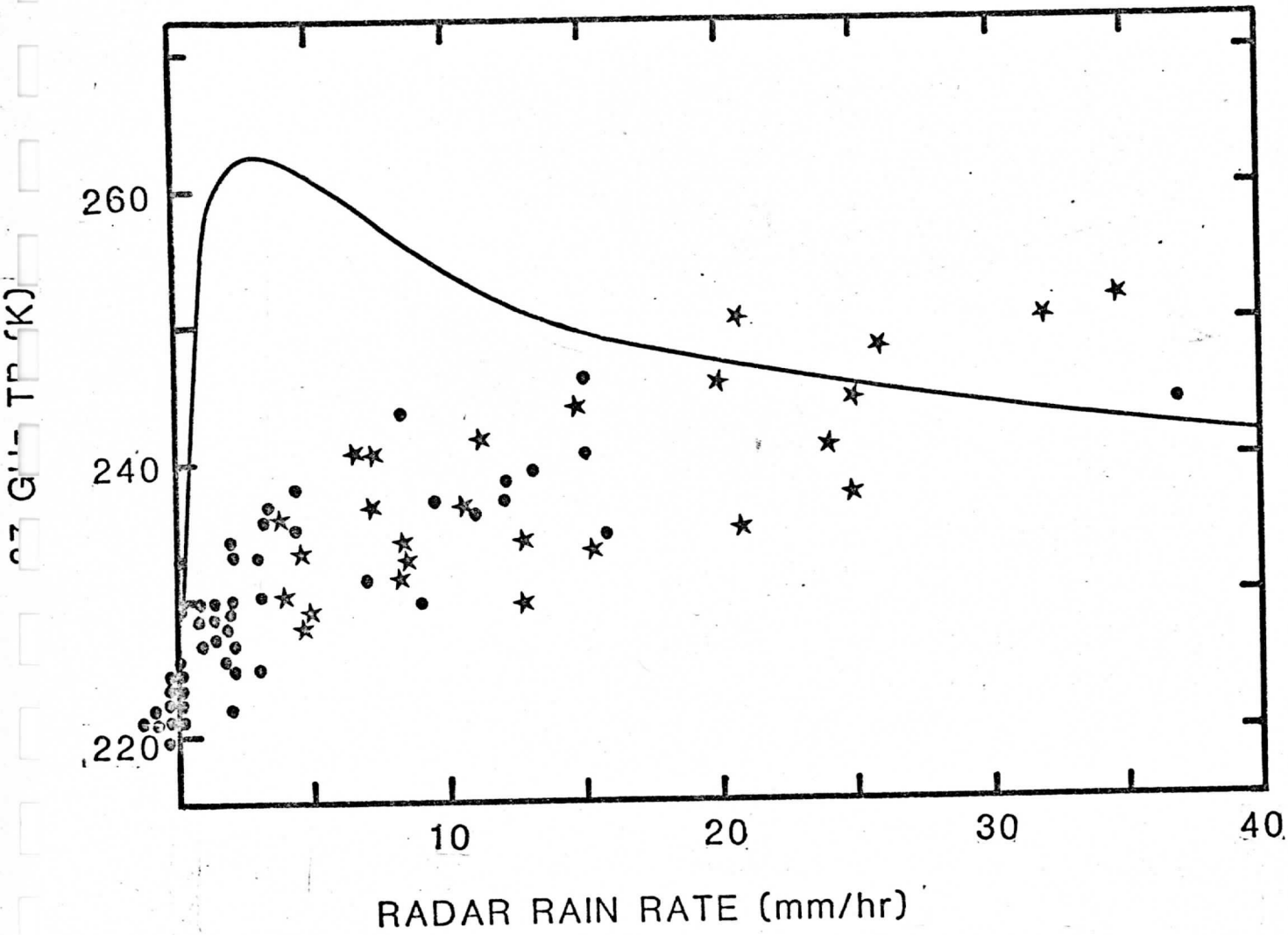


Fig. 4

Reprinted from Nature, Vol. 300, No. 5893, pp. 628-630, 16 December 1982


APPENDIX 5

# Rainfall over the Arabian Sea during the onset of the 1979 monsoon

**David W. Martin & Michael R. Howland**

Space Science and Engineering Center, The University of Wisconsin-Madison, Madison, Wisconsin 53706, USA

**One path to understanding the summer monsoon of south-east Asia lies through its regimes of rain. There the main scales of interest range, on the small side, down at least to component rainstorms: that is, extending over hundreds of kilometres and lasting about a day. On the large side, interest might be extended to include the whole quasi-planetary monsoon system, although here, for practical reasons, the limits are taken to be 1 week and several thousands of kilometres. The main branch of the summer monsoon forms over the Arabian Sea. The rainfall of this sea, roughly 3,000 km in its dimensions, is known to us from about 40 coastal stations, mostly in India, plus six instrumented islands and the reports of seagoing ships. The ships stay mainly in a few lanes and in any case only record the frequency of rain, not the amount. Thus, even taken all together, these reports are hardly adequate for building a picture of the monsoon rains. We report here a new technique for inferring daily rainfall from visible or IR images obtained by a geostationary satellite, applied in a simplified form to the Arabian Sea during the onset of the 1979 summer monsoon. The rain area estimated increased spectacularly (from 1 to 14%) over a 1-week period coincident with the appearance of the Somali jet and development of the onset vortex.**

Some scientists have exploited low-orbiting satellite observations of the Arabian Sea: C. S. Ramage, using visible imagery (personal communication), and Kidder and Vonder Haar and Rao *et al.*, using microwave data[1,2]. In each, the scale of the estimates—5 days or more—is too long to be of much use in portraying the monsoon through its development.

The 1979 Monsoon Experiment, which had an Arabian Sea component, may afford the best opportunity yet to build an evolutionary picture of the onset rains. The basis for this claim is the Indian Ocean Geostationary Operational Environmental Satellite (GOES IO). This satellite, positioned over the Equator

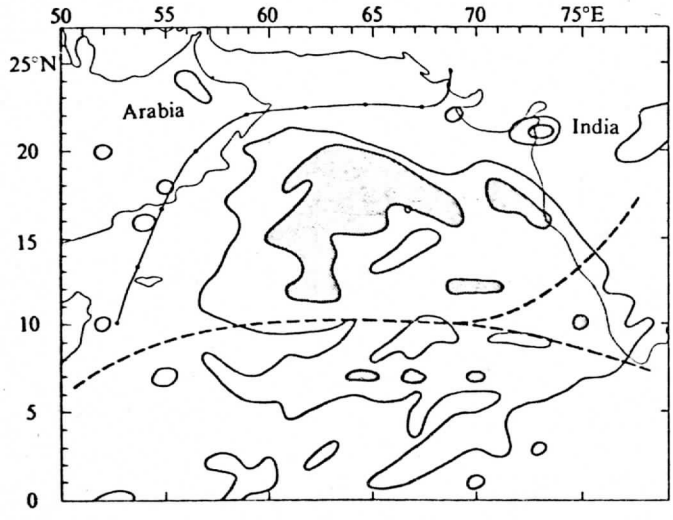


**Fig. 1** Rain frequency for 17 June 1979. Stippling marks the grid points where rain was registered at least once during the day. The darker stippling shows where the heavy rain class was recorded at least once. Also shown are the axis of the Somali jet (dashed line) and the centre of the onset vortex (circle, at 16° N, 67° E), both from ref. 7 and the edge of the monsoon inversion (knotted line), from ref. 9.

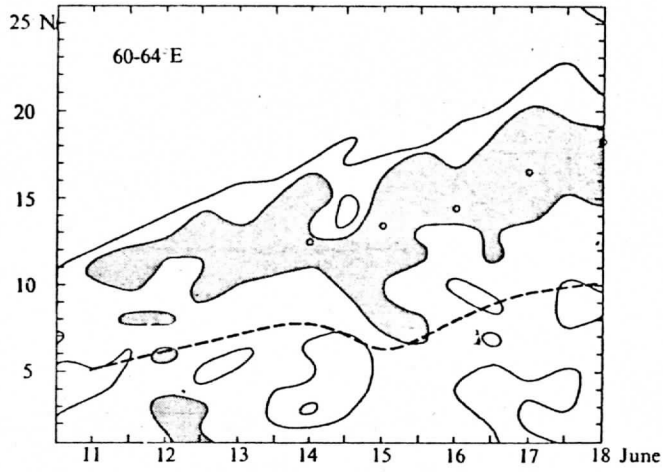


**Fig. 2** Time–latitude section of rain frequency averaged over a strip from 60 to 64° E. The convention is the same as for Fig. 1.

at 60 °E, returned a visible and/or IR image, of 1–8 km resolution, once in almost every hour of the days from 11 to 21 June, a period which coincides almost perfectly with the onset of the 1979 monsoon.

To map daily rainfall over the Arabian Sea as the 1979 summer monsoon became established, drawing on several studies (see refs 3 and 4), we hypothesize the following: (1) four rainrates (nil, light, moderate and heavy) can be inferred consistently at any hour from a sequence of hourly visible or IR images; (2) the nil-rate class predominates; (3) most nil and heavy cases can be decided solely on the basis of brightness; (4) time change of brightness and pattern are important in the remaining cases; (5) most of the data in a single image are redundant; and (6) visible and IR data are complementary.

One special constraint follows from the enormous volume of data generated by the GOES IO imaging instrument; we cannot look at every element of every picture. In fact, this kind of problem could only be addressed by training a machine to take repeated measurements and make simple decisions.

The approach that has been taken is to imagine a network of gauges, distributed over the basin of the Arabian Sea. For each hour at each gauge a meteorologist, assisted by a computer, infers from satellite pictures whether the rainfall was light, moderate, heavy or nonexistent. The sum over 24 h of these rainrate class assignments yields an estimate $\hat{R}$ of the daily rainfall $R$. Thus, if $\hat{r}_i$, $i = 0, 1, 2, 3$, is the estimate of hourly rainfall attributed to the $i$th rainrate class and $f_i$ is the frequency of the $i$th rainrate class over 24 h,

$$R \approx \hat{R} = f_0\hat{r}_0 + f_1\hat{r}_1 + f_2\hat{r}_2 + f_3\hat{r}_3$$

or, since $\hat{r}_0 \approx 0$

$$\hat{R} = f_1\hat{r}_1 + f_2\hat{r}_2 + f_3\hat{r}_3$$

Each $\hat{r}$ is a constant to be determined by multivariate least-squares regression of $\hat{r}$ on $R$, where $R$ is measured by a gauge or radar.

Rain is estimated from a sequence of Earth-located (navigated), registered satellite pictures, each image of the sequence being spaced an hour or so from the others. There may be an IR sequence and a visible sequence or either alone. Images are displayed and analysed on the University of Wisconsin Man-computer Interactive Data Access System, McIDAS[5].

Rain has been estimated by this so-called grid history technique for the area from the Equator to 28° N and from 50° E to 79° E. Initially, the resolution of the grid across this area was 0.5°. It has since been relaxed to 1°. Eight days have been processed, 11–18 June 1979.

Applications of this technique to parts of the South China Sea and the eastern Atlantic Ocean when gauges or radars were present suggest values for the coefficients in the ratio of 1 : 4 : 10.

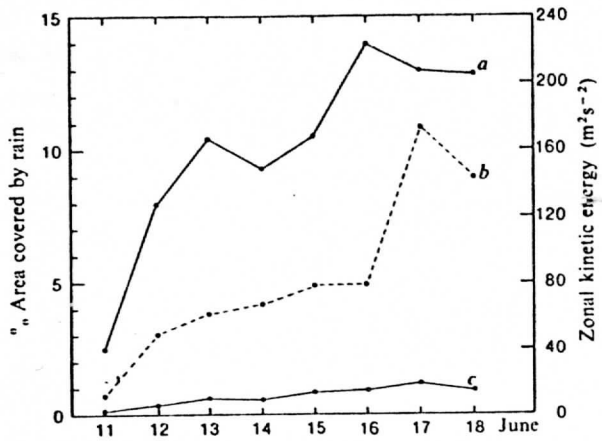


**Fig. 3** Rain coverage over the Arabian Sea from 11 to 18 June. Each point is an average over the hours from 00.00 to 23.00 GMT. *a*, All rain classes. *c*, Heavy rain class only. *b*, Values of area-averaged zonal kinetic energy, from ref. 8.

So far it has not been possible to acquire enough ground observations of rain around the Arabian Sea to run the regression there. Thus, only rain class frequencies are presented here.

A photographic view of rain frequency for 17 June 1979 is shown in Fig. 1. At this stage of the monsoon, rain was extensive over the Arabian Sea but largely absent over India. A band of mostly light to moderate rain, centred near 7° N, angled north and north-west along the Malabar coast of India, then merged with a large mass of mostly heavy rain in the north-central part of the Arabian Sea. The Somali jet bisected the rain area between the upper and lower masses, and the edge of the rain region lay 200–400 km east and south of the edge of the monsoon inversion.

Time changes in rain class frequency averaged across a longitudinal strip through the centre of the Arabian Sea (60–64° E) are shown in Fig. 2. Quite consistently, the heavier rain occurred on the north side of the rain area, to the left of the axis of the jet. The rain area spread steadily northwards, at ~150 km day$^{-1}$, or twice as fast as the northward movement of the jet axis.

It is expected from simple jet stream dynamics[6] that over the Arabian Sea, rain would be heaviest to the right of the axis of the Somali jet. The departure observed here is apparently due to low level convergence occurring with the onset vortex, a cyclone which first appears on 14 June in the 850-mbar analyses of the atlas of Krishnamurti *et al.*[7] The possibility has been suggested[8] that the onset vortex received kinetic energy through baroclinic processes (as well as barotropic processes), perhaps even during its formation. Figures 1 and 2 tend to confirm this, by showing first, a concentration of rain—implying ascent and release of latent heat—in the north-west semicircle of the storm, which available temperatures and winds indicate was the warmer half between 850 and 700 mbar, and second, the presence of heavy rain at least 2 days before the vortex was detectable in low level winds.

For the Arabian Sea as a whole, the percentage coverage by rain of light, moderate or heavy rain classes is shown in Fig. 3. The change over these eight days is remarkable: from 1% on 11 June to 14% on 18 June. The contribution of the heavy rain class to this growth is also shown in Fig. 3, from 0 to 1%. For heavy rain especially, the coverage curves closely parallel changes observed by Krishnamurti *et al.*[8] in zonal kinetic energy averaged over the Arabian Sea, suggesting that the convective response of the atmosphere to accelerations of the low level flow was relatively fast.

We conclude that the technique described here can provide information on the changing pattern of rainfall over the Arabian Sea through the onset phase of the summer monsoon. The precise limits of its accuracy remain to be established.

During the 1979 onset a near-equatorial belt of rainfall spread northwards across the centre of the Arabian Sea. Heavy rains developed, in association with an onset vortex, on the north flank of the Somali jet and moved north as the jet moved north.

This work was supported by the NSF under grant no. ATM-7920850.

Received 16 August; accepted 25 October 1982.

1. Kidder, S. Q. & Vonder Haar, T. H. *J. geophys. Res.* **82**, 2083–2086 (1977).
2. Rao, M. S. V., Abbott, W. V. III & Theon, J. S. *Satellite-Derived Global Oceanic Rainfall Atlas (1973 and 1974)* (NASA SP-410, Washington DC, 1976).
3. Barrett, E. C. & Martin, D. W. *The Use of Satellite Data in Rainfall Monitoring*, 102–123 (Academic, London, 1981).
4. Lovejoy, S. & Austin, G. L. *Atmos.–Ocean* **17**, 77–92 (1979).
5. Chatters, G. C. & Suomi, V. E. *IEEE Trans. Geosci. Electron.* **GE-13**, 137–146 (1975).
6. Uccellini, L. W. & Johnson, D. R. *Mon. Weath. Rev.* **107**, 682–703 (1979).
7. Krishnamurti, T. N., Ardanuy, P., Ramanathan, Y. & Pasch, P. *Quick Look Summer MONEX Atlas, Pt II. The Onset Phase*, 205 (Florida State University, Tallahassee, 1979).
8. Krishnamurti, T. N., Ardanuy, P., Ramanathan, Y. & Pasch, P. *Mon. Weath. Rev.* **109**, 344–363 (1981).
9. Narayanan, M. S. & Rao, B. M. *Nature* **294**, 546–548 (1981).